BIOCHEMISTRY
including biophysical chemistry & molecular biology

Article

pubs.acs.org/biochemistry

Molecular Dynamics Simulations of Binding Modes between Methylene Blue and DNA with Alternating GC and AT Sequences

Juan J. Nogueira* and Leticia González

Institute of Theoretical Chemistry, University of Vienna, Währinger Strasse 17 A-1090 Vienna, Austria

Supporting Information

ABSTRACT: The understanding of interactions between small molecules and DNA is crucial to design new anticancer drugs targeted to DNA. Methylene blue (MB) is a phenothiazinium dye that has shown promising results in photodynamic therapy treatment. The noncovalent binding of methylene blue to DNA was experimentally and theoretically analyzed in the past, but certain features of the binding mode are still not clear. In this work, force field molecular dynamics simulations were performed to simulate the binding of methylene blue to alternating GC and AT sequences at two different ionic strengths. External, intercalative, minor groove, and major groove binding modes are discussed based on energetic and structural analyses. External and major groove complexes were found to be unstable structures, although for poly(dA-dT) the major groove binding mode cannot be discarded, especially at high ionic strengths. Minor groove and intercalative binding leads to stable adducts. The most energetically favorable orientation of the dye inside the minor groove is different for the two DNA sequences because of the different balances between the DNA deformation energy and the dye/DNA interaction energy. The intercalative binding is the most important interaction mode. The dye undergoes rotational transitions inside the intercalative pocket for both DNA sequences giving rise to three dye/DNA adducts that have different energetic and structural features. This rotational motion explains the different behavior found in experiments for the GC and AT nucleic acids at different ionic strengths.

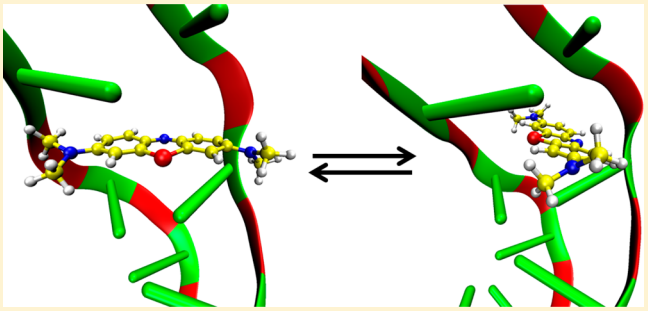

Anticancer therapies are often based on induction of DNA damage[1,2] because tumor cells are very prone to have deficits in the DNA repair mechanisms, and thus they are more likely to acquire genomic damage in comparison with normal cells. Therefore, the understanding of the types of interactions that take place between small molecules and DNA is of great interest in the design of new and more efficient anticancer agents. The binding of drugs to nucleic acids may take place by both covalent[3] and noncovalent interactions.[4]

Three binding modes exist[4,5] in which molecules can be noncovalently attached to DNA: (i) electrostatic binding, (ii) groove binding, and (iii) intercalative binding. Electrostatic (or external) binding usually occurs for too large cationic molecules that are not able to fit into the internal binding pockets of DNA. The drug interacts with DNA along the exterior of the helix, and the complex is dominated by Coulomb interactions between the cationic species and the negatively charged phosphate backbone. Groove binders are often formed by unfused aromatic ring systems that are connected by flexible chains that allow the drug to fit perfectly into the groove and to undergo van der Waals and/or hydrogen bond interactions with the helix. Large molecules usually are noncovalently associated to the major groove, while small molecules prefer to be placed into the minor groove. Intercalation is important for planar fused-ring aromatic molecules because the nucleic bases of DNA are arranged in an almost coplanar configuration, which allows strong π-stacking interactions with the drug. The above classification is very general, and thus many molecules noncovalently bind to DNA by more complex mechanisms[6] or by more than one interaction mode.[7]

Methylene blue (MB) is a phenothiazinium dye that is known to interact with DNA.[8−13] MB has received a lot of attention because it has shown promising applications in photodynamic therapy (PDT) for tumor[14−16] and microbial infection treatment.[17,18] In PDT, a photosensitive compound accumulates in tumors, and it is excited by low-energy light in the presence of ground state molecular oxygen.[19,20] Upon activation, the photosensitizer is promoted to excited states, and then several mechanisms that lead to photooxidative injuries in cell components may take place. The interaction of the drug with the biological environment, and in particular with DNA, is expected to influence the PDT mechanism since the photochemical properties of this type of compounds are strongly affected by the environmental conditions. For example, the intersystem crossing of MB and chlorophyll dyes was found to be enhanced upon the addition of molecular oxygen,[21] and absorption and emission spectra of MB have shown a

Received: January 16, 2014
Revised: March 21, 2014
Published: March 24, 2014

hypochromic effect in the presence of increasing amounts of DNA.[13] Thus, a comprehensive study of the interaction types that govern the photosensitizer/DNA adduct formation is required to provide information at the atomistic level of the PDT mechanism.

Several spectroscopic experiments were performed to analyze the binding mode between MB and DNA.[8−13] The general conclusion from these studies is that intercalation is the predominant binding mode, but somewhat more specific conclusions can be extracted from the literature. Analysis of absorption spectra for MB/polynucleotide systems[11] has shown that binding of MB to polynucleotide poly(dG-dC) is slightly stronger than to poly(dA-dT). This can be rationalized by recognizing that the GC base pair is more polar than AT,[22] and therefore the induced dipole in the intercalated dye is larger when it interacts with poly(dG-dC).[8] Linear and circular dichroism measurements[9] have concluded that MB can be intercalated in calf-thymus DNA by two different modes depending on the salt concentration. At low ionic strength, the orientation of the long axis of MB is parallel to the averaged long axis of the two flanking base pairs due to the strong stacking interactions. However, when the ionic strength is increased, cations interact with the negatively charged phosphate groups of DNA, and the repulsion between these counterion clouds of the phosphates and the positive dimethylamino groups of MB becomes important. This unfavorable situation is alleviated by the rotation of MB to a perpendicular orientation. Some of these conclusions were extended in a more recent spectroscopic work[12] where the MB/DNA binding mode was investigated for the polynucleotides poly(dG-dC), poly(dA-dT), poly(dG)poly(dC), poly(dA)poly(dT), and calf-thymus DNA at different ionic strengths. Two of the main findings of this work are (i) binding mode of MB to poly(dG-dC) is intercalative and insensitive to the ionic strength; the intercalation is suggested to take place in two different base pair steps 5′-G-C-3′ and 5′-C-G-3′ or in two different MB angular orientations. (ii) MB/poly(dA-dT) interaction is mainly intercalative at low salt concentration, but increasing ionic strength MB partially moves to a second external binding site which is suggested to be placed in the major groove.

Molecular mechanics conformational search and energy minimization have been carried out[23−25] to model the interaction of MB with DNA. Two decamers with alternating GC and AT sequences and different salt concentrations ranging from 0 to 2.0 M were investigated. These theoretical simulations nicely fit many of the experimental findings. However, three important issues are not completely clear from these studies. First, simulations predict that electrostatic stabilization of MB/DNA adducts owing to the increase of salt concentration is higher for the minor groove binding than for intercalation for both GC[25] and AT[24] sequences. The lower stabilization for intercalation is likely related with the fact that the charge density of DNA decreases after the complexation in the intercalative pocket due to the prolongation of the double strand.[24] This behavior leads to comparable binding energies for the intercalative and minor groove MB/DNA complexes at high salt concentrations. However, spectroscopic measurements[12] have shown that the binding mode for poly(dG-dC) is purely intercalative regardless the ionic strength. One important source of error in the simulations[24,25] could be that the treatment of the solvent and salt effects are only included as a correction to the energy of the final optimized structures. In other words, the conformational search and energy minimization procedure were performed in a vacuum, and therefore the structure of the MB/DNA adducts do not change with the salt concentration. Second, small energy differences between several MB/DNA complexes with different binding modes were found in the simulations,[23−25] and, as mentioned above, transitions between parallel and perpendicular intercalative structures could explain some spectroscopic measurements.[9] This suggests that more than one structure could exist under certain conditions, but a time-dependent picture of the system is necessary to corroborate it. Finally, molecular mechanics optimizations[23,24] have shown that MB is inserted into the minor groove of GC and AT decamers with its methyl groups facing outside the groove, giving rise to similar structures for the GC and AT nucleic acids. Moreover, the binding energies of MB interacting with both DNA sequences are very similar for the entire range of ionic strengths theoretically analyzed. However, more recent Monte Carlo simulations[26] performed by the same authors have revealed that the MB orientation in the minor groove depends on the DNA sequence. The later result is likely more reasonable since poly(dG-dC) and poly(dA-dT) present a different chemical environment inside the minor groove, and thus some differences between the MB/GC and MB/AT minor groove structures are expected. DNA sequence-dependent orientation within the minor groove was observed for the Hoechst 33258 drug by X-ray measurements.[27]

Using force field molecular dynamics (MD) simulations, the noncovalent binding of MB to two DNA sequences and for two different ionic strengths was analyzed in this work. Our goal is to perform energetic and structural analyses that will allow us to unravel some unclear features of the MB/DNA binding mode. The rest of the paper is organized as follows. Materials and Methods is devoted to the computational details of the initial structure generation, the MD simulations, and the methods employed in the analyses. In Results and Discussion, the results for the different binding modes are discussed, with particular emphasis on the minor groove and intercalative complexes, which are the most important binding structures for MB/DNA. The discussion about the intercalative binding mode is organized in four different subsections. Finally, conclusions are discussed the last section.

MATERIALS AND METHODS

Initial Structures. MB was noncovalently bonded to two dodecamers with alternating GC and AT sequences. Two ionic strengths, 0 and 1.0 M, were investigated. A schematic representation of the two polynucleotides is shown in Scheme 1 with the base numeration which will be useful later in the discussion of the results. We generated eight different initial

Scheme 1. Representation of the Sequence Context for (a) poly(dG-dC) and (b) poly(dA-dT)

(a)

5′	G1	C2	G3	C4	G5	C6	G7	C8	G9	C10	G11	C12	3′
3′	C24	G23	C22	G21	C20	G19	C18	G17	C16	G15	C14	G13	5′

(b)

5′	A1	T2	A3	T4	A5	T6	A7	T8	A9	T10	A11	T12	3′
3′	T24	A23	T22	A21	T20	A19	T18	A17	T16	A15	T14	A13	5′

dx.doi.org/10.1021/bi500068z | Biochemistry 2014, 53, 2391−2412

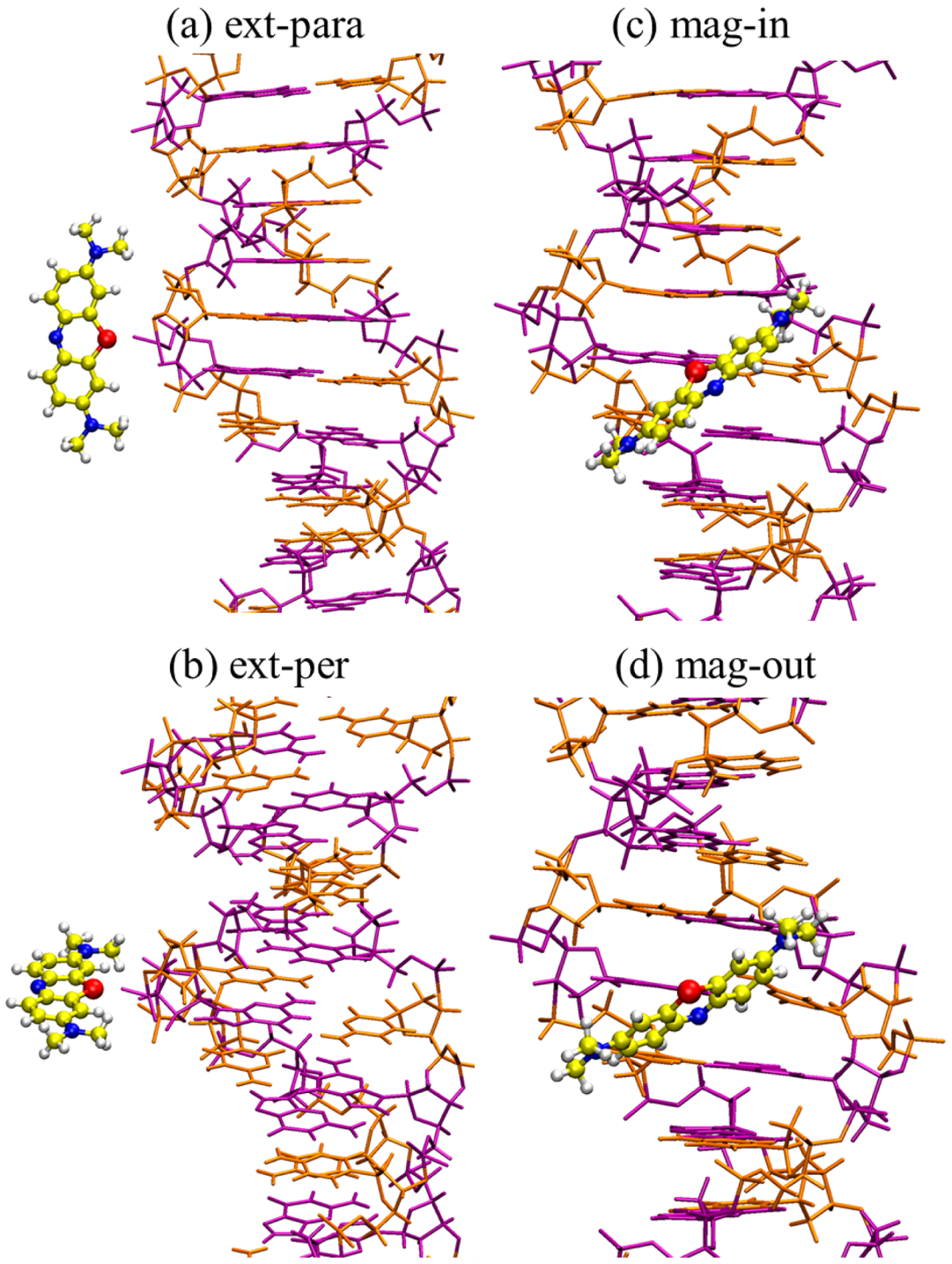

Figure 1. Initial structures of external binding complexes with the long axis of MB (a) parallel (ext-para) and (b) perpendicular (ext-per) to the helical axis, and major groove binding complexes with the dimethylamino groups pointing (c) inside (mag-in) and (d) outside (mag-out) the groove. Color atoms and residues: yellow for C, blue for N, red for S, white for H, purple for guanine, and orange for cytosine.

structures for each DNA sequence and ionic strength in which MB was placed in four binding sites, namely, external phosphate, intercalation pocket, major groove, and minor groove. For each of the four binding modes, MB was bind to DNA with two different orientations, as can be seen in Figures 1 and 2. In the case of external binding, the long axis of MB was chosen to be parallel (ext-para) and perpendicular (ext-per) to the helical axis. For the intercalative structures, MB was inserted into the base pair steps 5′-C-G-3′ and 5′-T-A-3′ for the GC and AT sequences, respectively, with the cyclic ring system of the dye being perpendicular to the helical axis. In one of the intercalative structures, the long axis of MB forms an angle of 0° with the averaged long axis of the flanking basis pairs (int-sym), and in the second structure MB is right-handed rotated by 140° around the helical axis (int-gau). These two orientations were selected because the potential energy surface shows two deep minima at these angles.[23] Following the notation of previous theoretical works,[23−25] we will refer to the two intercalative binding modes as symmetric intercalation (int-sym) and gauche intercalation (int-gau) for angles of 0° and

dx.doi.org/10.1021/bi500068z | *Biochemistry* 2014, 53, 2391−2412

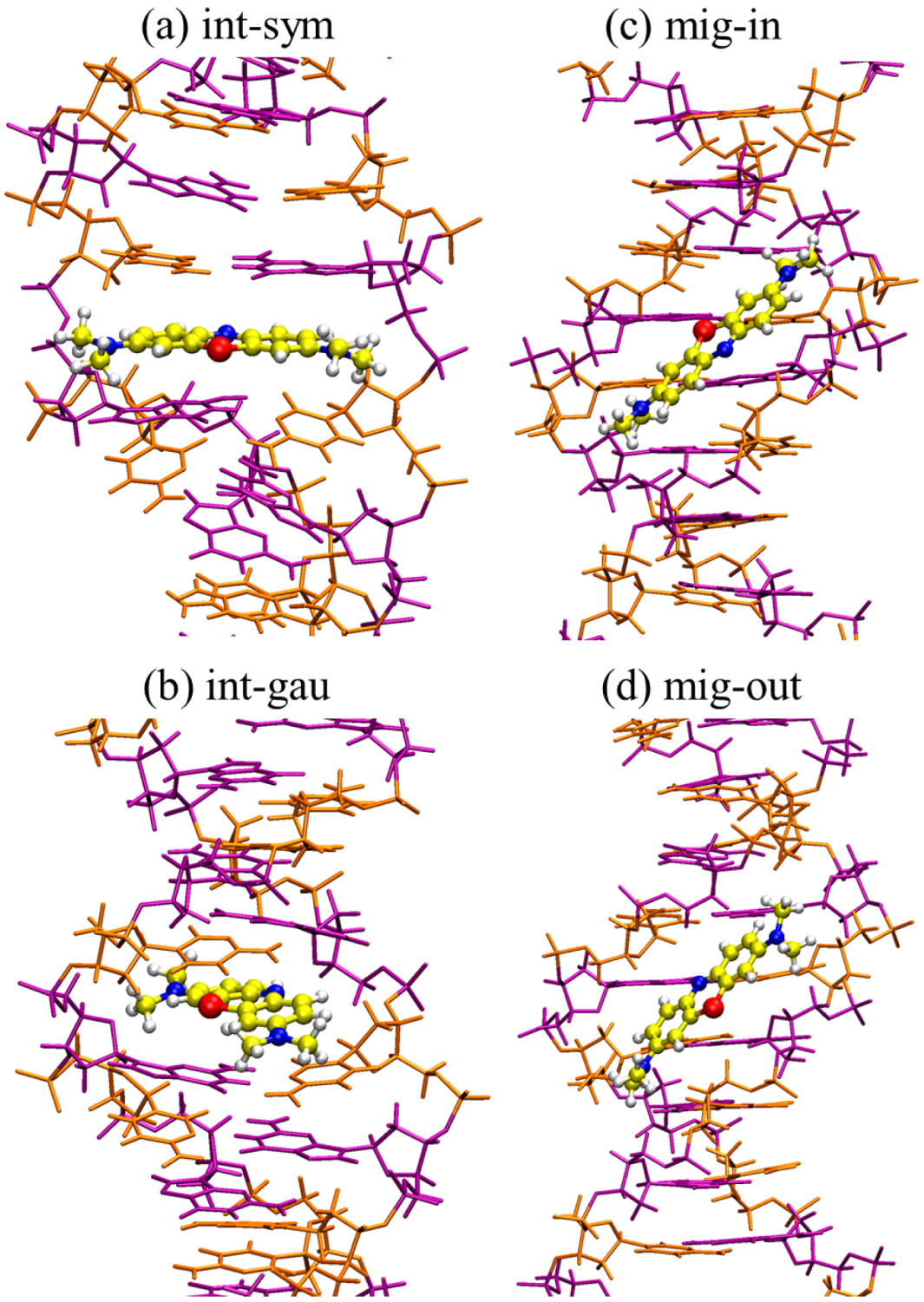

Figure 2. Initial structures of intercalative binding complexes with the long axis of MB (a) parallel (int-sym) and (b) rotated by 140° (int-gau) with respect to the averaged long axis of the flanking basis pairs, and minor groove binding complexes with the dimethylamino groups pointing (c) inside (mig-in) and (d) outside (mig-out) the groove. Color atoms and residues: yellow for C, blue for N, red for S, white for H, purple for guanine, and orange for cytosine.

140°, respectively. Regarding the minor and major groove bindings, the dye was located into the grooves with the dimethylamino groups pointing inside (mig-in and mag-in) and outside (mig-out and mag-out) the groove. The DNA sequences were generated with the nucleic acid builder (NAB) module of AmberTools13,[28] and then the MB dye was inserted manually into the corresponding binding site.

The initial MB/DNA geometries were neutralized with Na^+ ions using the LEAP module of AmberTools13.[28] Then, the neutralized systems were fully solvated by a periodic truncated octahedral box of water molecules described by the TIP3P model[29] extended to a distance of 10 Å from any solute atom. Since the ion concentration in these structures is very low, we will refer to these ionic conditions as 0 M ionic strength. The

dx.doi.org/10.1021/bi500068z | *Biochemistry* 2014, 53, 2391−2412

ionic strength of 1.0 M was established by adding randomly the appropriate amount of Na^+/Cl^- pairs to the solvation box. In total, the simulated systems consist of around 15000−20000 atoms.

Simulation Details. We performed force field MD simulations using the NAMD 2.9 package.[30] The potential parameters for the dye were taken from the general AMBER force field (GAFF) for organic molecules;[31] the ff99 set of parameters[32] with the bsc0 modification[33] was employed for the nucleic acids. The restrained electrostatic potential (RESP) charges of MB were calculated at the Hartree−Fock/6-31G* level of theory, to be consistent with the rest of the force field, using the Gaussian09 software.[34] The calculated atomic charges of MB and the atom types from the GAFF force field are displayed in Figure S1 of the Supporting Information. The complete set of parameters for MB in prmtop format is listed in Appendix A of the Supporting Information.

After the initial configuration construction explained in the previous section, we performed the next protocol for the simulations. In the first stage, the MB and DNA molecules were fixed, and water and ion positions were minimized with the conjugate gradient method for 10 000 steps. In a second step, the entire system was minimized for 20 000 steps. After minimization, a slow constant volume (NVT) heating to 300 K over 20 ps was performed with a time step of 1 fs. Then, the density of the system was equilibrated in constant pressure and temperature conditions (NPT) for 100 ps. Finally, the production simulations were run in the NPT ensemble using Langevin dynamics to maintain a temperature of 300 K and pressure of 1 atm. The SHAKE algorithm was used to restrain the lengths of all bonds that involve hydrogen atoms, allowing the increase of the time step up to 2 fs. The simulations of external and major groove binding structures were extended up to 10 ns (5×10^6 time steps), while the minor groove and intercalative binding modes were simulated for 40 ns (2×10^7 time steps). Throughout the entire simulation protocol, the Coulomb and van der Waals contributions of the potential were truncated at 10 Å. The Coulomb part was evaluated by means of the particle mesh Ewald (PME) method with a grid spacing of 1 Å in each direction, a fourth-order interpolation and a direct sum tolerance of 10^{-6}. Snapshots of the production simulations were recorded every 4 ps, and the second half of the simulation was employed for energetic and structural analyses in the case of minor groove and intercalative binding. External and major groove binding simulations did not provide stable adducts; therefore, the analyses were carried out over the time for which the dye is interacting with the nucleic acid. In some cases, the interaction time is very short to extract quantitative conclusions; therefore, only a qualitative picture can be described.

Analysis Methods. Curves+,[35] a nucleic acid conformational analysis program, was used for analyzing several structural parameters of DNA when it is interacting with MB. Intra- and interbase pair rotational and translational parameters, the total helical axis bend, and the width and depth of the minor and major groove were computed. The first and the last base pairs in the nucleic acid sequence were excluded to avoid unrealistic torsions due to end effects. VMD[36] was used to visualize the trajectories generated and to evaluate interaction energies between residues of the MB/DNA adducts by means of the NAMDenergy plugin. The presence of hydrogen bonds between MB and the DNA sequence was analyzed with the help of the CPPTRAJ program[37] of AmberTools13.[28] The hydrogen bond analysis was based on a distance cutoff of 3.5 Å between the donor and acceptor and an angular cutoff of 120° among the donor, hydrogen, and acceptor.

Binding free energies of MB/DNA complexes were calculated with the molecular mechanics Poisson−Boltzmann surface area (MM-PBSA) approach[38−40] as implemented in AMBER12.[28] The binding energy is calculated by subtracting the free energies of the solvated unbound nucleic acid G(DNA) and dye G(MB) from the free energy of the solvated complex G(MB/DNA):

$$\Delta G_{\text{bind}} = G(\text{MB/DNA}) - (G(\text{MB}) + G(\text{DNA})) \quad (1)$$

Each of the terms on the right-hand side of eq 1 is computed according to

$$G(\text{X}) = E_{\text{gas}}(\text{X}) + \Delta G_{\text{solv}}(\text{X}) - TS(\text{X}) \quad (2)$$

The term E_{gas}(X) refers to the gas-phase energy of the system X, and it is approximated by the molecular mechanics energy of the system, determined from the force field used in the simulations. E_{gas}(X) is the sum of the bonded and nonbonded (Coulomb and van der Waals) energies:

$$E_{\text{gas}}(\text{X}) = E_{\text{bonded}}(\text{X}) + E_{\text{Coul}}(\text{X}) + E_{\text{vdW}}(\text{X}) \quad (3)$$

The solvation free energy $\Delta G_{\text{solv}}(X)$ of eq 2 is calculated using an implicit solvent model and is decomposed into two contributions, a polar and a nonpolar one:

$$\Delta G_{\text{solv}}(\text{X}) = \Delta G_{\text{polar}}(\text{X}) + \Delta G_{\text{nonpolar}}(\text{X}) \quad (4)$$

The calculation of the polar part ΔG_{polar}(X) is based on the finite difference solution to the Poisson−Boltzmann equation. The nonpolar contribution of the solvation energy $\Delta G_{\text{nonpolar}}$(X) is assumed proportional to the solvent-accessible surface area (SASA) and is computed as the sum of a disfavorable energy resulting from solute−solvent repulsive interactions and the cavity formation for the solute within the solvent, and a favorable energy resulting from dispersion attractive interactions between solute and solvent molecules.[41]

The term $-TS(X)$ of eq 2 is the solute entropy and can be estimated using a rigid-rotor harmonic oscillator approximation and applying normal-mode analysis or quasi-harmonic analysis. In our case, the entropic term was neglected for two reasons. First, our goal is not to compute the absolute value of the binding free energies but to make relative comparisons between different binding modes. As all calculations are performed for the same system (MB/DNA), the decrease of entropy of the ligand after complexation will be similar for the different binding modes. Second, it has been reported that the entropy change upon ligand binding is overestimated by normal-mode analysis and a good convergence of the entropy is hardly reached by quasi-harmonic analysis.[42]

The pairwise energy decomposition implemented in the MM-PBSA algorithm of AMBER12[28] allows reorganizing the previous equations. Accordingly, the binding free energy can be expressed as the sum of the MB deformation energy E_{def} (MB), DNA deformation energy E_{def} (DNA), intermolecular binding energy E_{inter} (MB/DNA), and nonpolar part of the solvation energy $\Delta G_{\text{nonpolar}}$:

$$\Delta G_{\text{bind}} = E_{\text{def}}(\text{MB}) + E_{\text{def}}(\text{DNA}) + E_{\text{int er}}(\text{MB/DNA}) + \Delta G_{\text{nonpolar}} \quad (5)$$

dx.doi.org/10.1021/bi500068z | Biochemistry 2014, 53, 2391−2412

Scheme 2. Time Evolution of MB Throughout the External and Major Groove Binding Mode Simulations[a]

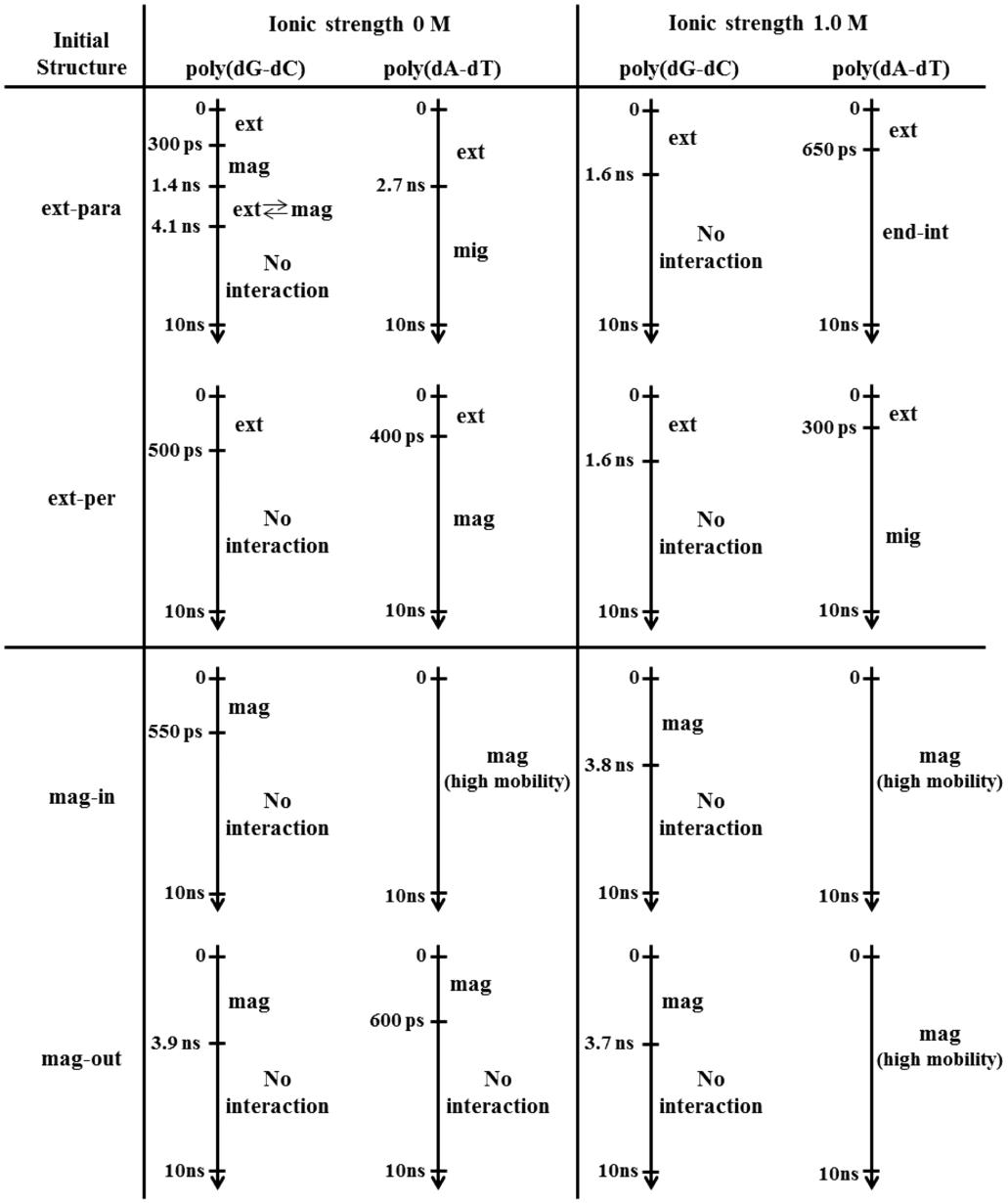

[a]Time axes are only indicative (not quantitative).

where each of the first three terms is computed as the sum of the variation of the gas-phase energy after complexation and the polar part of the solvation energy:

$$E_{\mathrm{def}}(\mathrm{MB}) = \Delta E_{\mathrm{gas}}(\mathrm{MB}) + \Delta G_{\mathrm{polar}}(\mathrm{MB}) \quad (6)$$

$$E_{\mathrm{def}}(\mathrm{DNA}) = \Delta E_{\mathrm{gas}}(\mathrm{DNA}) + \Delta G_{\mathrm{polar}}(\mathrm{DNA}) \quad (7)$$

$$E_{\mathrm{int\ er}}(\mathrm{MB/DNA}) = E_{\mathrm{gas}}(\mathrm{MB/DNA}) + \Delta G_{\mathrm{polar}}(\mathrm{MB/DNA}) \quad (8)$$

The nonpolar part of the solvation energy $\Delta G_{\mathrm{nonpolar}}$ is currently not decomposable. However, it is much smaller than the polar contribution, and therefore the conclusions will not be significantly affected by its absence in eqs 6−8.

We have employed the multiple trajectory protocol (MTP) using separate simulations for MB, DNA, and MB/DNA complex to extract the bound and unbound terms of eq 1. This approach is more appropriate than the single trajectory protocol (STP) when the ligand and/or the receptor suffer strong conformational changes after complexation.[40] In our case, important differences in the DNA structure are observed when MB interacts with the different binding sites of the double strand.

Convergence of the Simulations. The simulations of the external and major groove binding modes did not provide stable complexes as will be discussed below; therefore, a steady state was not reached. Minor groove and intercalative bindings were the only interaction modes that led to stable structures. The root mean squared deviation (RMSD) of the DNA and MB heavy atoms was calculated against the starting structure for those trajectories which showed strong MB/DNA binding. Figures S1 and S2 of the Supporting Information show the RMSD for the minor groove and intercalative binding mode

dx.doi.org/10.1021/bi500068z | Biochemistry 2014, 53, 2391−2412

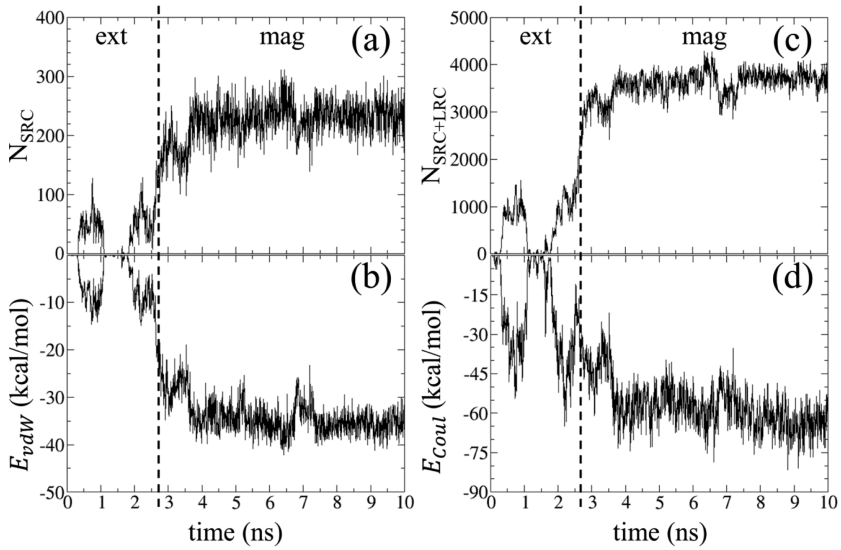

Figure 3. Time evolution of (a) the number of short-range contacts N_{SRC} (cutoff 4 Å), (b) MB/DNA van der Waals energy E_{vdW}, (c) the number of total (short and long-range) contacts $N_{SRC+LRC}$ (cutoff 8 Å), and (d) MB/DNA Coulomb energy E_{Coul} for poly(dA-dT) with initial geometry ext-para at ionic strength 0 M.

simulations, respectively. Uniform RMSD fluctuations are observed virtually over the whole simulation time for the four minor groove simulations at ionic strength 0 M. At high ionic strength, the first half part of the simulations presents important RMSD oscillations, especially for the mig-out orientations. In such cases, the visualization of the trajectories reveals that the dye travels though the minor groove of the double strand during the first half fraction of the simulation, and after ~20 ns the system adopts an equilibrated structure.

In the case of the intercalative structures, the situation is different. Some of the simulations underwent transitions between the symmetric and gauche orientations as will be discussed in the Intercalative Binding section. Such rotational motion of MB inside the intercalative pocket induces large DNA structural changes that do not allow the system to achieve an equilibrated geometry. Even for those trajectories for which the dye preserves the initial orientation the whole simulation time, several rotations that result in frustrated transitions are observed. Comparison of Figures S2 and S3 shows that the fluctuations of the RMSDs are larger for the intercalative geometries than those for the minor groove ones. To make a more quantitative comparison, the maximum RMSD amplitude was defined as the difference between the largest and the smallest RMSD value during the last 20 ns of simulation. The average of the maximum RMSD amplitudes for all the minor groove and intercalative trajectories is 2.5 Å and 3.0 Å, respectively. This means that the convergence of the intercalative binding simulations is not as good as that of the minor groove binding simulations. This out of equilibrium situation is expected when the DNA abruptly changes its structure throughout the dynamics due to transitions between different binding modes.[43]

RESULTS AND DISCUSSION

Initially, MD simulations were carried out for 10 ns for the four binding modes specified before. External and major groove MB/DNA adducts were unstable throughout the simulation time as will be discussed later. In contrast, the MB dye was found to strongly bind to DNA into the minor groove and the intercalative pockets. For this reason, the trajectories that simulate these two more important binding modes were extended up to 40 ns, so that better statistics were achieved from the simulations. The obtained results are organized in five different sections. In the first two sections, the most important features of the unstable external and major groove configurations are presented. The third presents the binding free energies for the minor groove and the intercalative complexes and discusses the general trends comparing the results with the experiments. Finally, in the fourth and fifth sections an extensive analysis based on energy decompositions and DNA structural features is performed for the minor groove and intercalative binding modes, respectively.

External Binding. In general, external binding complexes have not been suggested as stable structures for the interaction of MB with DNA sequences by experimental measurements.[8−13] To the best of our knowledge, there is only one experimental work,[44] based on spectroscopic and electrochemical measurements, that revealed that the MB/DNA interactive model is the electrostatic binding mode. However, in that work the MB dye was loaded inside the hydrophobic cavity of a β-cyclodextrin, and thus the interaction with DNA is likely affected by the presence of the macromolecule by avoiding the access to some of the binding pockets of DNA.

Our simulations agree with the experimental findings of refs 8−13 showing that external MB/DNA adducts dissociate during the simulation time for the eight initial conditions studied, that is, parallel and perpendicular MB orientations with respect to the helical axis of poly(dG-dC) and poly(dA-dT) at ionic strengths 0 and 1.0 M. The interaction time between MB and the phosphate groups is in the range between 300 ps and 2.7 ns depending on the DNA sequence and the ionic strength. After the dissociation, the dye leaves the helix or goes to another interaction site. Scheme 2 collects the different binding sites where MB is placed along the simulations and the time at which transitions occur. To characterize the simulation time at which the transitions take place the number of contacts between the atoms of MB and DNA were calculated using an atom-to-atom cutoff of 8 Å. This cutoff distance is larger than usual values employed in the literature[45,46] (3−5 Å) because the external binding mode is dominated by long-range

dx.doi.org/10.1021/bi500068z | *Biochemistry* 2014, 53, 2391−2412

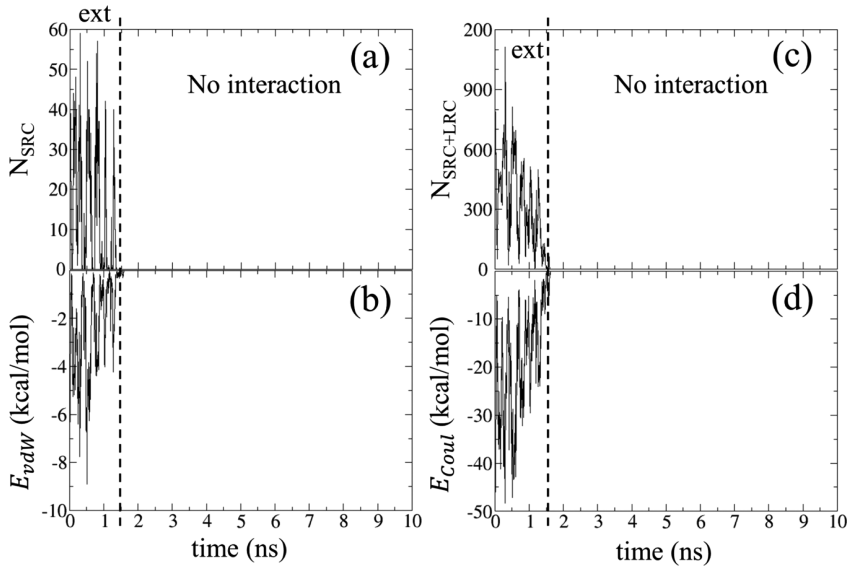

Figure 4. Time evolution of (a) the number of short-range contacts N_{SRC} (cutoff 4 Å), (b) MB/DNA van der Waals energy E_{vdW}, (c) the number of total (short and long-range) contacts $N_{SRC+LRC}$ (cutoff 8 Å), and (d) MB/DNA Coulomb energy E_{Coul} for poly(dG-dC) with initial geometry ext-per at ionic strength 1.0 M.

Table 1. MB/DNA Gas-Phase Coulomb E_{Coul} (MB/DNA) and van der Waals E_{vdW} (MB/DNA) Interaction Energies in kcal/mol for External Complexes at Ionic Strengths 0 and 1.0 M

		ionic strength 0 M		ionic strength 1.0 M	
initial structure	energy contribution[a]	poly(dG-dC)	poly(dA-dT)	poly(dG-dC)	poly(dA-dT)
ext-para	E_{vdW} (MB/DNA)	−0.7	−5.4	−0.3	−2.9
	E_{Coul} (MB/DNA)	−8.0 (92)[b]	−21.9 (80)	−4.8 (94)	−11.7 (80)
ext-per	E_{vdW} (MB/DNA)	−0.2	−17.2	−2.2	−9.8
	E_{Coul} (MB/DNA)	−4.0 (95)	−46.0 (73)	−18.7 (90)	−34.1 (78)

[a]Energies are averaged over the interaction time between MB and DNA (see text). [b]Percentage with respect to the total gas-phase interaction energy.

Coulomb interactions. Smaller values of cutoff are chosen when short-range van der Waals interactions are analyzed. Hydrogen atoms are usually excluded[45,46] for describing the number of contacts because they are taken into account separately by hydrogen bond analyses. Since the formation of hydrogen bonds is not possible when the dye is interacting with the double strand in external positions, hydrogen atoms were also included in our analysis for counting the number of contacts. Moreover, the number of contacts between MB and DNA were also calculated with a smaller cutoff of 4 Å. The choice of these two different cutoff values (4 Å and 8 Å) allows computing the number of short-range contacts N_{SRC} and the number of total contacts $N_{SRC+LRC}$ (short and long-range contacts), which correlate with van der Waals E_{vdW} (MB/DNA) and Coulomb E_{Coul} (MB/DNA) interaction energies, respectively.

Figures 3 and 4 display the variation of N_{SRC}, $N_{SRC+LRC}$, E_{vdW} (MB/DNA), and E_{Coul} (MB/DNA) throughout the dynamics for poly(dA-dT) with initial geometry ext-para at ionic strength 0 M and for poly(dG-dC) with initial geometry ext-per at ionic strength 1.0 M. These simulations were chosen because they represent the two situations observed in the dynamics, that is, the transition between the external position and other binding site (major groove) and diffusion of the dye from the external position to the bulk solvent. When the dye leaves the external position of the helix and diffuses toward the solvent, the number of contacts decreases drastically until vanishing (Figure 4a,c). We consider that there is not interaction between the dye and DNA when $N_{SRC+LRC} = 0$. If the dye undergoes a transition between the external position and the minor or major groove, the number of contacts increases rapidly (Figure 3a,c). The time step at which the increase of $N_{SRC+LRC}$ happens is chosen as the transition time in Scheme 2. Figures 3 and 4 also show the expected correlation between N_{SRC} and E_{vdW} (MB/DNA) and between $N_{SRC+LRC}$ and E_{Coul} (MB/DNA); that is, the intermolecular energies become more (less) attractive with increasing (decreasing) the number of contacts.

The E_{Coul} (MB/DNA) and E_{vdW} (MB/DNA) contributions to the MB/DNA total gas-phase interaction energy were computed for all the external initial conditions. Table 1 shows the energies averaged over the frames in which the dye is interacting with the DNA helix in the external position. Since the system adopts the external binding mode only for 2.7 ns at most (Scheme 2), the energies of Table 1 must be interpreted with care because the number of time steps is not large enough to obtain an accurate analysis. One of the consequences of that is the wide range of energy values computed for E_{Coul} (MB/DNA) (between −4.0 and −46.0 kcal/mol) and E_{vdW} (MB/DNA) (between −0.2 and −9.8 kcal/mol). The only consistent trend extracted from Table 1 is the percentage of the total energy that comes from Coulomb and van der Waals contributions. It was found that the ∼93% (∼78%) of the MB/DNA total gas-phase interaction energy is due to Coulomb interactions for the GC (AT) sequence. Therefore, the external binding mode is clearly dominated by long-range Coulomb

interactions for both nucleic acids. Additional conclusions from Table 1 can be unwary.

It is interesting to notice that for one of the simulations (initial geometry ext-para for the AT sequence at ionic strength 1.0 M) the dye moves from the external site to the end of the double strand and interacts with the last A12-T13 base pair by a stacking mode. However, this end-intercalative configuration is unrealistic and is achieved in the simulations due to the finite length of the DNA molecule. In conclusion, on the basis of previous experimental research and on our simulation results, the external binding can be discarded as a favorable binding mode between MB and DNA.

Major Groove Binding. Spectroscopic experiments[12] show that MB may bind to an alternating AT polynucleotide in one of the grooves at high salt concentrations. Such experiments, however, cannot distinguish the specific groove. On the basis of the fact that the dye could potentially be involved in hydrogen bonding to the free NH_2 group of the major groove but this is not possible in the minor groove, the major groove interaction has been postulated as the most probable binding mode. However, theoretical simulations[24] have shown that minor groove binding is clearly favored over major groove binding for a wide range of salt concentrations. The conclusion obtained from the experiments that the major groove is the preferred binding site is a conjecture based on chemical intuition. In contrast, simulations predicted that the interaction of the dye with the minor groove has a larger binding energy than that with the major groove. The fact that the simulated angle[24] between the long axis of MB and the helical axis of DNA qualitatively agrees with the experimental value[12] supports the validity of the simulations.

Our simulations show two different behaviors for the GC and AT sequences regarding the major groove interaction (Scheme 2). In the case of poly(dG-dC), none of the four different initial conditions analyzed here leads to a stable major groove complex. For all the cases, the dye goes away from the nucleic acid after a certain period of interaction. This interaction time is around 4 ns for three of the four simulations and 550 ps for the remaining trajectory. As for the external binding simulations, the interaction time was calculated by assuming that the dye has left the major groove when $N_{SRC+LRC} = 0$. This assumption probably overestimates the interaction time because the dye could be considered to be outside the groove before all interatomic distances between MB and DNA are larger than 8 Å. In any case, MB interacts longer with poly(dG-dC) in the major groove than in external positions (Scheme 2). The longest period of interaction found in the simulations of GC was 1.6 ns for the external binding and 3.9 ns for the major groove binding.

In contrast, the situation is different for the MB/poly(dA-dT) adducts. The dye stays in the major groove for the entire simulation in three of the four initial conditions. Despite the long interaction time, the MB/DNA adduct is characterized by highly variable positions and orientations of MB inside the groove and by excursions of MB toward the external phosphate backbone. As an example, Figure 5b depicts the time evolution of the angle formed by the short axis of MB v_{short}(MB) and the helical axis of DNA v_{helix} computed at the T6-A19 base pair level (see Figure 5a for definition of the axes), for the initial geometry mag-in and high salt concentration. As can be seen, the angle oscillates virtually between 0 and 180°, which points to a large rotational motion of the dye inside the groove. This behavior indicates that there is no clear energy minimum that

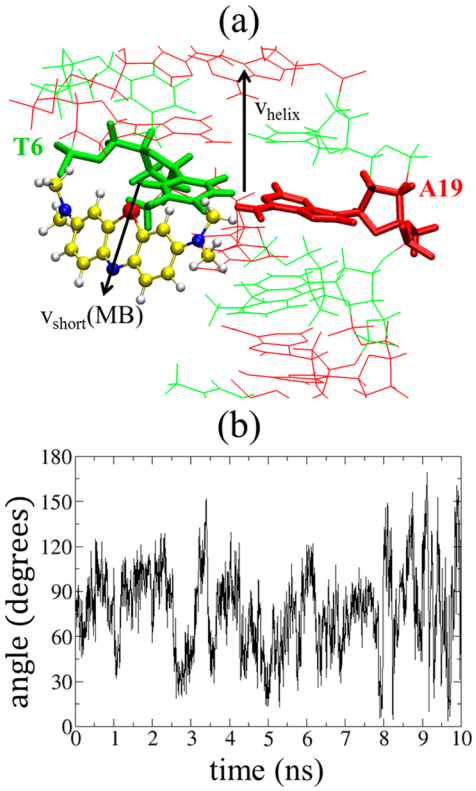

Figure 5. (a) Short axis of MB v_{short}(MB) and helical axis v_{helix} at the T6-A19 base pair level and (b) time evolution of the angle formed v_{short}(MB) and v_{helix} along the simulation for the mag-in initial geometry in the AT sequence at ionic strength 1.0 M. Color atoms and residues: yellow for C, blue for N, red for S, white for H, green for thymine, and red for adenine.

stabilizes the formation of the MB/DNA complex in the major groove. Such high mobility of the dye inside the major groove also was found in previous Monte Carlo simulations.[26]

Gas-phase van der Waals E_{vdW} (MB/DNA) and Coulomb E_{Coul} (MB/DNA) interaction energies between the dye and the DNA sequences were computed over the interaction time and are listed in Table 2. The simulations with very short MB/DNA interaction times will be excluded from the analyses of the present section. In particular, the discarded trajectories are those for poly(dG-dC) with initial structure mag-in at ionic strength 0 M (interaction time 550 ps) and poly(dA-dT) with initial structure mag-out at ionic strength 0 M (interaction time 600 ps).

At low salt concentration, the MB/DNA total gas-phase interaction is clearly stronger for the AT sequence (−46.6 kcal/mol) than that for the GC sequence (−25.1 kcal/mol). Both E_{vdW} (MB/DNA) and E_{Coul} (MB/DNA) energies are larger for poly(dA-dT), especially the short-range contribution (−16.8 kcal/mol vs −5.1 kcal/mol). In the version of the AMBER force field[31−33] that we are employing in our simulations, there is not an explicit term that defines the hydrogen bond interaction, but they are considered in the attractive term of the Lennard-Jones potential (which describes the van der Waals interactions). Therefore, the large difference observed in E_{vdW} (MB/DNA) between poly(dG-dC) and poly(dA-dT) at low ionic strength could be explained by different hydrogen bond formation.

Both DNA sequences are able to form hydrogen bonds between their NH_2 groups, which lie into the major groove, and

dx.doi.org/10.1021/bi500068z | Biochemistry 2014, 53, 2391−2412

Table 2. MB/DNA Gas-Phase Coulomb E_{Coul} (MB/DNA) and van der Waals E_{vdW} (MB/DNA) Interaction Energies in kcal/mol for Major Groove Complexes at Ionic Strengths 0 and 1.0 M

		ionic strength 0 M		ionic strength 1.0 M	
initial structure	energy contribution[a]	poly(dG-dC)	poly(dA-dT)	poly(dG-dC)	poly(dA-dT)
mag-in	E_{vdW} (MB/DNA)	−8.4	−16.8	−11.8	−15.1
	E_{Coul} (MB/DNA)	−24.2 (74)[b]	−29.8 (64)	−29.7 (72)	−23.1 (61)
mag-out	E_{vdW} (MB/DNA)	−5.1	−4.1	−14.3	−19.8
	E_{Coul} (MB/DNA)	−20.0 (80)	−32.4 (89)	−39.3 (73)	−25.4 (56)

[a]Energies are averaged over the interaction time between MB and DNA (see text). [b]Percentage with respect to the total gas-phase interaction energy.

the aromatic N atom of MB as seen in Figure 6. The N4 and N6 atoms of cytosine and adenine, respectively, are the hydrogen donor atoms (D) and the aromatic N atom of MB is the hydrogen acceptor (A). Hydrogen bonding is possible only if the aromatic N atom of the dye points toward the major groove (mag-out orientation). However, because of the high rotational mobility of the dye inside the major groove (Figure 5b) the mag-out orientation was achieved for all the initial conditions during several periods of time of the simulations. Therefore, hydrogen bond formation was always observed to a greater or lesser extent.

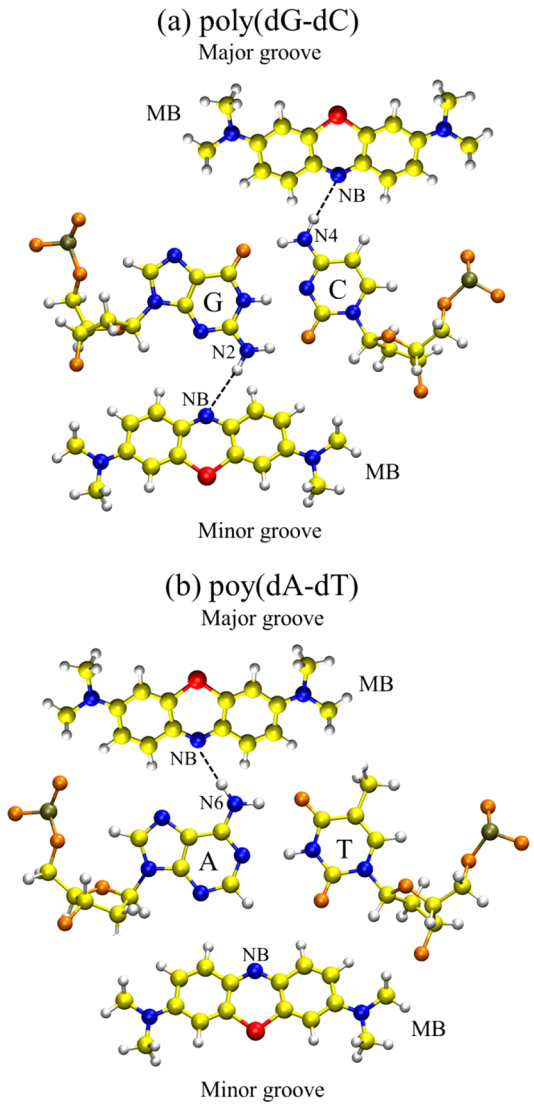

Figure 6. Schematic representation of hydrogen bond formation in the minor and major grooves between MB and (a) the GC base pair and (b) the AT base pair. Color atoms: yellow for C, blue for N, red for S, orange for O, tan for P, and white for H.

Table 3 lists the distance R_{DA} between the D and A atoms, the angle θ_{DHA} formed by D—H—A and the fraction of time $x_{t(H)}$ over which the hydrogen bond is present with respect to the total time of interaction between the MB and the major groove. The hydrogen bond lifetimes $x_{t(H)}$ explain the significant differences found in E_{vdW} (MB/DNA) for the GC (−5.1 kcal/mol) and AT (−16.8 kcal/mol) sequences at ionic strength 0 M. The hydrogen bond is present only during the 1.3% of the interaction time for GC, while the percentage increases up to 31.7% for AT.

At high ionic strength, both E_{vdW} (MB/DNA) and E_{Coul} (MB/DNA) are more attractive than those at low salt concentration for poly(dG-dC) (Table 2). The increase of the short-range interaction is reflected in $x_{t(H)}$. At these conditions, the hydrogen bonds exist during the 36% and 19% of the interaction time for the initial geometries mag-in and mag-out, respectively. The hydrogen bond lifetimes also increase for poly(dA-dT) from 32% at low ionic strength to 52% and 76% for the initial structures mag-in and mag-out, respectively, at high ionic strength. However, in that case the increment of E_{vdW} (MB/DNA) is only observed for the initial geometry mag-out (−19.8 kcal/mol), while for mag-in the value of E_{vdW} (MB/DNA) is slightly smaller (−15.1 kcal/mol) than that for low ionic strength (−16.8 kcal/mol). This behavior is not surprising because the E_{vdW} (MB/DNA) term does not describe exclusively the hydrogen bond interactions but all the short-range interactions. Therefore, a perfect correlation between E_{vdW} (MB/DNA) and $x_{t(H)}$ is not expected.

Comparison of the energies of Tables 1 and 2 reveals that the contribution of the E_{Coul} (MB/DNA) term to the MB/DNA total interaction energy is more important for the external binding mode than for the major groove binding mode. The percentage of E_{Coul} (MB/DNA) decreases from ∼93% (∼75%) for the external binding in GC (AT) to ∼75% (∼60%) for the major groove binding in GC (AT). This is a consequence of hydrogen bonding in the major groove complexes which is taken into account in the E_{vdW} (MB/DNA) energy term. Therefore, although Coulomb interactions are still dominant in the major groove adducts, the hydrogen bonds contribute significantly to the MB/DNA total gas-phase interaction energy.

Finally, our simulations conclude that major groove binding is relatively stable over the whole simulation time only for the AT sequence. The formation of hydrogen bonds between MB and the NH_2 groups inside the major groove facilitates the stabilization of the complexes. But even for the AT sequence, a clearly stable MB/DNA configuration is not reached. High

dx.doi.org/10.1021/bi500068z | Biochemistry 2014, 53, 2391−2412

Table 3. Information about the Hydrogen Bonds Formed in the Major Groove Simulations between NB and N4 (GC) or N6 (AT)[a]

	ionic strength 0 M				ionic strength 1.0 M			
	poly(dG-dC)		poly(dA-dT)		poly(dG-dC)		poly(dA-dT)	
	mag-in	mag-out	mag-in	mag-out	mag-in	mag-out	mag-in	mag-out
R_{DA}	3.18	3.29	3.17	3.37	3.18	3.18	3.20	3.17
θ_{DHA}	129.9	142.2	145.5	138.9	156.7	154.3	144.2	145.5
$x_{t(H)}$	0.04	0.01	0.32	0.02	0.36	0.19	0.52	0.76

[a]See also Figure 6 for definition of the atoms. R_{DA} is the separation (Å) between the hydrogen donor (N4 or N6) and the hydrogen acceptor (NB), θ_{DHA} is the angle formed by N4(N6)—H—NB (deg), and $x_{t(H)}$ is the fraction of time that the hydrogen bond exists with respect to the total interaction time between MB and DNA.

Table 4. Binding Free Energies (kcal/mol) of MB/DNA Complexes for Minor Groove and Intercalative Structures at Ionic Strengths 0 and 1.0 M

	ionic strength 0 M				ionic strength 1.0 M			
	poly(dG-dC)		poly(dA-dT)		poly(dG-dC)		poly(dA-dT)	
initial structure	energy[a]	MD structure[b]	energy	MD structure	energy	MD structure	energy	MD structure
mig-in	−6.2	mig-in	−5.7	mig-in	−7.3	mig-in	−8.8	mig-in
mig-out	−7.3	mig-out	−1.2	mig-out	−9.4	mig-out	−0.9	mig-out
int-sym	−9.6	int-sym/int-gau	−13.5	int-sym	−16.5	int-sym	−8.9	int-gau
int-gau	−18.1 (−15.7)[c]	int-sym	−3.0	int-sym/int-gau	−18.3 (−16.1)[c]	int-sym/int-gau	−8.5	int-gau

[a]The standard error of the mean for all binding energies is ~0.6 kcal/mol. [b]MB/DNA geometries observed over the last 20 ns of the simulation. See also Scheme 3. [c]Binding energy if the analysis is performed over the last 28 ns.

rotational and translational motion of the dye inside the groove was observed for all the initial conditions.

Binding Energies. As discussed before, major groove and external binding simulations did not lead to stable complexes; therefore, binding free energies were calculated only for the minor groove and intercalation adducts by the MM-PBSA method (see Analysis Methods section). Table 4 shows the energy values for the different initial conditions evaluated over the last 20 ns of the simulations.

For the alternating GC sequence, the most favorable binding energy corresponds to an intercalative complex regardless the ionic strength (−18.1 and −18.3 kcal/mol for salt concentration 0 and 1.0 M, respectively). In the case of the AT polynucleotide, the intercalative binding configuration is the most stable structure at salt concentration 0 M but with increasing the ionic strength the intercalative binding energy decreases from −13.5 to −8.9 kcal/mol so that it is comparable in magnitude to the minor groove binding energy (−8.8 kcal/mol). Thus, simulations predict that both structures may exist at high ionic strength conditions. The same trends for GC and AT polynucleotides have been observed in spectroscopic measurements.[12] The binding mode of MB to poly(dG-dC) was found to be intercalative and insensitive to the ionic strength. In the case of poly(dA-dT), intercalation is also the interactive mode at low ionic strength, but two different binding sites were detected at high ionic strength.[12]

Table 4 also shows that binding energies for the GC sequence are stronger than for AT for both minor groove and intercalative complexes and for both ionic strengths. Equilibrium constants for MB/DNA adduct formation determined by absorption spectroscopy[11] and previous molecular mechanics conformational calculations[24] also indicated a preference for the GC sequence.

Although the calculated binding energies nicely reproduce the experimental findings, conclusions must be made with care since the binding energies of intercalative complexes depends on the fragment of the simulation that is being analyzed. This dependence is related to transitions between symmetric and gauche geometries that take place during the simulations; that is, the initial geometry (int-sym or int-gau) is not conserved over the whole simulation. The geometries that are observed in the last 20 ns of the simulations are listed in Table 4, and a more detailed picture is shown in Scheme 3. The symmetric/gauche transitions will be analyzed in the Intercalative Binding section.

MB was initially inserted into the minor groove in two different orientations, with the dimethylamino groups directed inward (mig-in) and outward (mig-out) of the groove. MB exhibits strong attractive interactions with the two DNA sequences for both orientations, and the dye does not change its relative orientation during the 40 ns of the simulations. An interesting behavior is found by comparing the minor groove binding energies for poly(dG-dT) and poly(dA-dT). The relative stability of mig-in and mig-out orientations depends on the DNA sequence. Thus, for the GC polynucleotide, the mig-out orientation is energetically more favorable, while the mig-in configuration is the most stable for the AT sequence. This trend does not vary with ionic strength as seen in Table 4.

Minor Groove Binding. Binding energies of Table 4 show that minor groove complexes are stable structures for both GC and AT sequences. In addition, the initial orientation of MB does not change along the simulations as is shown in Scheme 3, indicating that mig-in and mig-out configurations are deep minima in the potential energy surface. Previous theoretical calculations[23,24] predicted that the most favorable binding energy is reached when the dye is inserted into the minor group with its dimethylamino groups facing outside the groove (mig-out), independently of the DNA sequence. However, later docking Monte Carlo simulations[26] performed by the same authors have shown different behaviors for the alternating GC and AT polynucleotides. They have observed that mig-in orientation is favored over mig-out for the AT sequence, while

dx.doi.org/10.1021/bi500068z | Biochemistry 2014, 53, 2391−2412

Scheme 3. Time Evolution of MB throughout the Minor Groove and Intercalative Binding Mode Simulations[a]

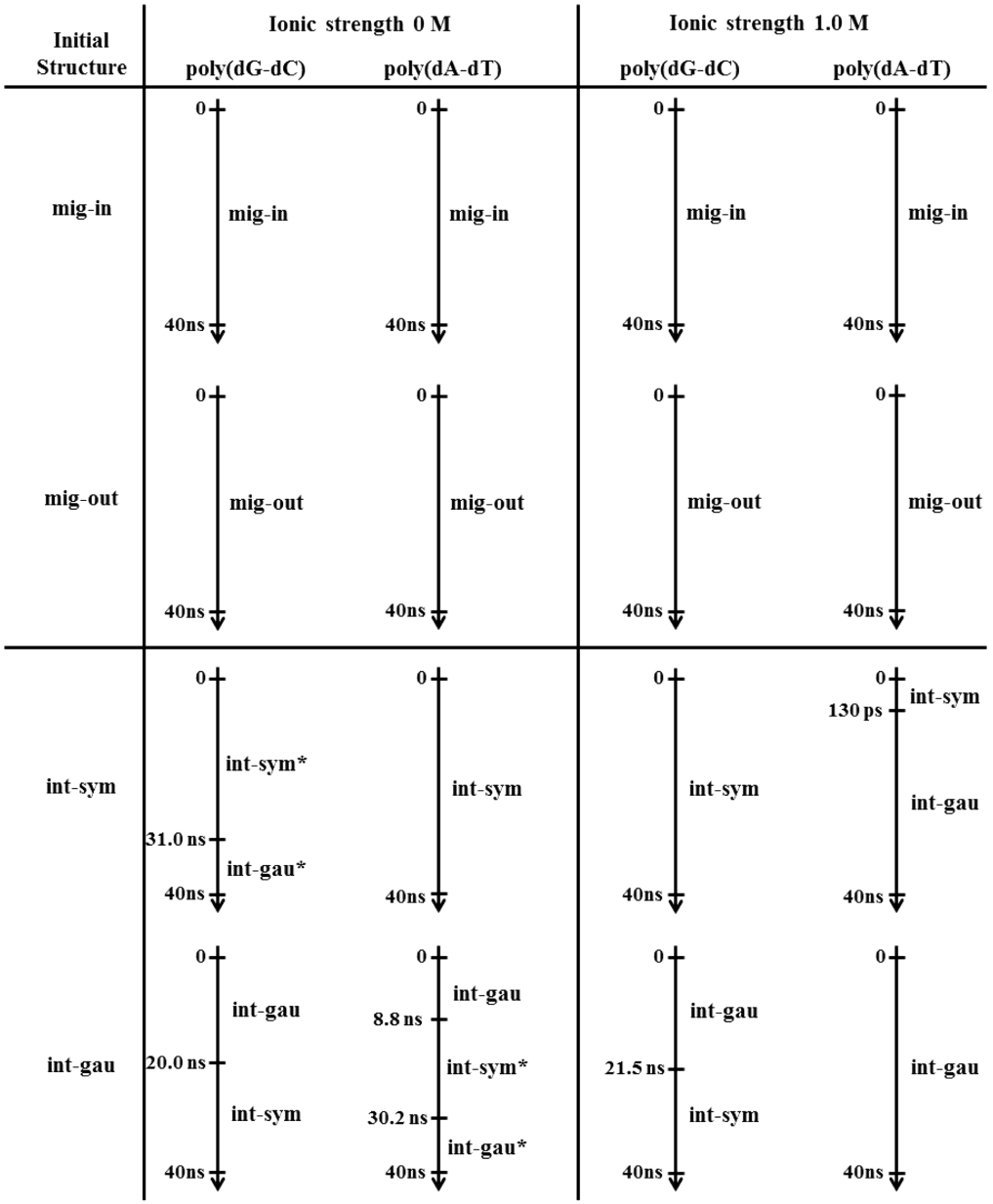

[a]Time axes are only indicative (not quantitative).

Table 5. Binding Free Energy Decomposition (kcal/mol) into MB Deformation Energy E_{def} (MB), DNA Deformation Energy E_{def} (DNA), Intermolecular Energy E_{inter} (MB/DNA), and Nonpolar Solvation Energy $\Delta G_{nonpolar}$ for the Minor Groove Complexes at Ionic Strengths 0 and 1.0 M

		ionic strength 0 M		ionic strength 1.0 M	
initial structure	energy contribution	poly(dG-dC)	poly(dA-dT)	poly(dG-dC)	poly(dA-dT)
mig-in	E_{def} (MB)	6.3	7.9	7.7	7.3
	E_{def} (DNA)	22.6	34.0	25.0	28.8
	E_{inter} (MB/DNA)	−53.4	−66.8	−58.0	−66.0
	$\Delta G_{nonpolar}$	18.3	19.2	17.9	21.1
mig-out	E_{def} (MB)	5.6	5.8	5.8	5.5
	E_{def} (DNA)	18.9	24.4	18.3	24.9
	E_{inter} (MB/DNA)	−49.8	−50.5	−50.4	−50.5
	$\Delta G_{nonpolar}$	18.0	19.1	16.9	19.2

the mig-out orientation was the only configuration found in the simulations with GC.

Our MD simulations agree with the more recent Monte Carlo results.[26] The mig-out orientation has the strongest

dx.doi.org/10.1021/bi500068z | Biochemistry 2014, 53, 2391−2412

Table 6. Decomposition of the Intermolecular Energy (kcal/mol) E_{inter} (MB/DNA) into Gas-Phase Coulomb E_{Coul} (MB/DNA) and van der Waals E_{vdW} (MB/DNA) Contributions and Polar Intermolecular Solvation Energy ΔG_{polar} (MB/DNA) for Minor Groove Complexes of GC and AT Sequences at Ionic Strengths 0 and 1.0 M[a]

		ionic strength 0 M		ionic strength 1.0 M	
initial structure	energy contribution	poly(dG-dC)	poly(dA-dT)	poly(dG-dC)	poly(dA-dT)
mig-in	E_{vdW} (MB/DNA)	−35.5	−42.6	−39.6	−42.6
	N_{SRC}	249	289	281	288
	E_{Coul} (MB/DNA)	−550.7	−549.4	−529.4	−551.2
	$N_{SRC+LRC}$	3905	4356	4216	4341
	ΔG_{polar} (MB/DNA)	532.8	525.2	511.0	527.8
mig-out	E_{vdW} (MB/DNA)	−34.9	−35.1	−35.6	−36.0
	N_{SRC}	232	228	240	233
	E_{Coul} (MB/DNA)	−535.1	−531.2	−525.0	−531.5
	$N_{SRC+LRC}$	3720	3577	3761	3673
	ΔG_{polar} (MB/DNA)	520.2	515.7	510.3	517.0

[a]The number of short-range N_{SRC} and total $N_{SRC+LRC}$ interatomic contacts between MB and DNA is also listed.

Table 7. Minor Groove Width and Depth (Å) of poly(dG-dC) and poly(dA-dT) after Minor Groove Binding of MB at Ionic Strengths 0 and 1.0 M[a]

		ionic strength 0 M		ionic strength 1.0 M	
initial structure	energy contribution	poly(dG-dC)	poly(dA-dT)	poly(dG-dC)	poly(dA-dT)
mig-in	width	6.44 (6.99)	5.77 (6.41)	6.83 (6.22)	5.67 (6.68)
	depth	5.29 (4.83)	4.58 (4.19)	4.90 (5.10)	4.57 (4.22)
mig-out	width	6.32 (6.99)	5.80 (6.41)	6.53 (6.22)	5.91 (6.68)
	depth	4.98 (4.83)	4.59 (4.19)	5.01 (5.10)	4.52 (4.22)

[a]The values of the free DNA sequences are shown in parentheses for comparison.

binding energy (−7.3 and −9.4 kcal/mol at ionic strengths 0 and 1.0 M, respectively) for poly(dG-dC), while the mig-in configuration is more favorable (−5.7 and −8.8 kcal/mol at ionic strengths 0 and 1.0 M, respectively) for poly(dA-dT). The energy decomposition according to eqs 5−8 for the minor groove simulations shown in Table 5 allows us to examine the most important energy contributions. As expected, the DNA deformation energy is larger for the mig-in orientation than for the mig-out orientation (about 4−10 kcal/mol depending on the DNA sequence and salt concentration). The bulky dimethylamino groups of MB induce large DNA structural changes when they point toward the groove.

For both poly(dG-dC) and poly(dA-dT), the mig-in orientation favors attractive MB/DNA intermolecular energy E_{inter} (MB/DNA) due to the larger number of MB/DNA contacts. As eq 8 reads, E_{inter} (MB/DNA) is the sum of the gas-phase intermolecular energy E_{gas} (MB/DNA) and intermolecular polar solvation energy ΔG_{polar} (MB/DNA). In turn, E_{gas} (MB/DNA) is composed of Coulomb E_{Coul} (MB/DNA) and van der Waals E_{vdW} (MB/DNA) interactions between the dye and the nucleic acids. These different contributions and the number of short-range N_{SRC} (cutoff 4 Å) and total $N_{SRC+LRC}$ (cutoff 8 Å) contacts averaged over the last 20 ns of simulation are listed in Table 6 for the mig-in and mig-out orientations. Both gas-phase energy contributions (Coulomb and van der Waals) are more favorable in the mig-in configurations for both DNA sequences, especially in the case of AT, making the mig-in configuration the most stable minor groove structure for poly(dA-dT). However, this attractive intermolecular energy is not strong enough to counteract the unfavorable DNA deformation energy in the case of the poly(dG-dC) sequence, so that the mig-out configuration presents the strongest binding energy at both salt concentrations.

As expected, N_{SRC} and $N_{SRC+LRC}$ nicely correlate with E_{vdW} (MB/DNA) and E_{Coul} (MB/DNA), respectively; that is, the mig-in orientation for both DNA sequences presents a larger amount of interatomic contacts than the mig-out orientation, and therefore stronger Coulomb and van der Waals energies. Comparison of the E_{vdW} (MB/DNA) and E_{Coul} (MB/DNA) energies reveals that the minor groove binding is dominated by Coulomb interactions. For all initial conditions investigated, E_{Coul} (MB/DNA) is always more than the 90% of the total gas-phase interaction energy.

In the mig-in orientation, $N_{SRC+LRC}$ is larger for AT than that for GC independently of the ionic strength (4356 vs 3905 at ionic strength 0 M and 4341 vs 4216 at ionic strength 1.0 M). This larger amount of contacts for poly(dA-dT) induces more attractive interactions. The total MB/DNA gas-phase interaction energy (E_{vdW} (MB/DNA) + E_{Coul} (MB/DNA)) is −586.2 kcal/mol for GC and −592.0 kcal/mol for AT at ionic strength 0 M, and −569.0 kcal/mol for GC and −593.8 kcal/mol for AT at ionic strength 1.0 M. These differences can be related to the fact that the guanine residues of the GC sequence have an NH_2 group lying in the minor groove which is not present in the AT sequence (Figure 6). Therefore, the higher steric effect inside the minor groove of GC disfavors the formation of MB/DNA interatomic contacts resulting in lower interaction energy.

Regarding the mig-out configuration, the aromatic N atom of MB forms a hydrogen bond with the NH_2 group of one of the guanine residues for poly(dG-dC) as Figure 6 displays. In particular, for the simulations performed at ionic strengths 0 and 1.0 M, the hydrogen bond is formed with the G7 and G17 residues, respectively. The hydrogen bond is present during the 90% (89%) of the simulation time with an average NB−N2 distance of 3.14 Å (3.15 Å) and an average NB−H—N2 angle of 157.9° (158.7°) for the structure at ionic strength 0 M (1.0

dx.doi.org/10.1021/bi500068z | Biochemistry 2014, 53, 2391−2412

M). However, this hydrogen bond has a minor effect on the intermolecular energy between MB and DNA since, as discussed in the previous paragraph, the MB/poly(dG-dC) gas-phase attraction is stronger for the mig-in configuration, for which the aromatic N atom of MB is oriented toward the solvent, and therefore hydrogen bond formation is not possible. Nevertheless, the mig-out configuration has the most favorable binding energy for the MB/poly(dG-dC) adduct (Table 4) owing to the complex balance of different energy contributions, in which the DNA deformation energy plays an important role (see Table 5). In the case of poly(dA-dT), the absence of hydrogen donors inside the minor groove precludes the formation of hydrogen bonds; the NH_2 donor group of the adenine residues lies inside the major groove (not in the minor groove).

The width and depth of the minor groove after complexation were analyzed and are listed in Table 7. The minor groove binding of MB induces an expected minor groove narrowing and deepening on the AT sequence independently of the ionic strength and on the GC sequence at low salt concentration. However, the minor groove is broadened and flattened at high ionic strength for poly(dG-dC), above all for the mig-in configuration. This increase of the minor groove width (from 6.22 Å to 6.83 Å) is originated by the high mobility of the dye inside the groove at high salt concentration. The mobility can be analyzed in terms of the angle formed by the short axis of MB and the helical axis of DNA (see definition of the axes in Figure 5a). Figure 7a,b compares the time evolution of this angle for the GC and AT polynucleotides at ionic strength 1.0 M. Angular values close to 0° or 180° produces large minor groove widening, while values around 90° inflicts the narrowing of the groove, as can be seen in Figure 7c. The mobility of the dye in the mig-in orientation is clearly higher for the GC sequence than for AT (Figure 7a). This agrees with the smaller MB/DNA gas-phase intermolecular energy for poly(dG-dC) in comparison to poly(dA-dT) observed in Table 6. The sum of the van der Waals and Coulomb contributions is −569.0 and −593.8 kcal/mol for GC and AT, respectively. This means that the attractive energy that the dye has to break to rotate inside the minor groove is smaller for the GC sequence, and therefore more mobility is favored. The rotation of the dye inside the groove is a consequence of the strong interactions between MB and the large amount of ions in the solvent. The difference on dye rotation between poly(dG-dC) and poly(dA-dT) is less important for the mig-out orientation (Figure 7b). In that case, the sum of the van der Waals and electrostatic energies is similar for both DNA sequences (−560.6 and −567.5 kcal/mol for GC and AT, respectively). These different minor groove structural variations with the ionic strength for GC and AT were not observed in previous molecular mechanics simulations.[23,24] As discussed above, in those simulations the effect of the solvent and salt concentration was taken into account solely to correct the energies of the final optimized geometries, and therefore the adduct structures could not change with the ionic strength.

Intercalative Binding. Intercalative binding has been predicted as the most important interaction mode by both experiments[8−13] and simulations.[23−25] The binding energies of Table 4 extracted from our simulations also show that the intercalative structures, in general, dominate the dynamics of the system. The combination of the GAFF[31] force field for MB and the bsc0 modification[33] of the ff99 set of parameters[32] for DNA does not account explicitly for the π-stacking interactions,

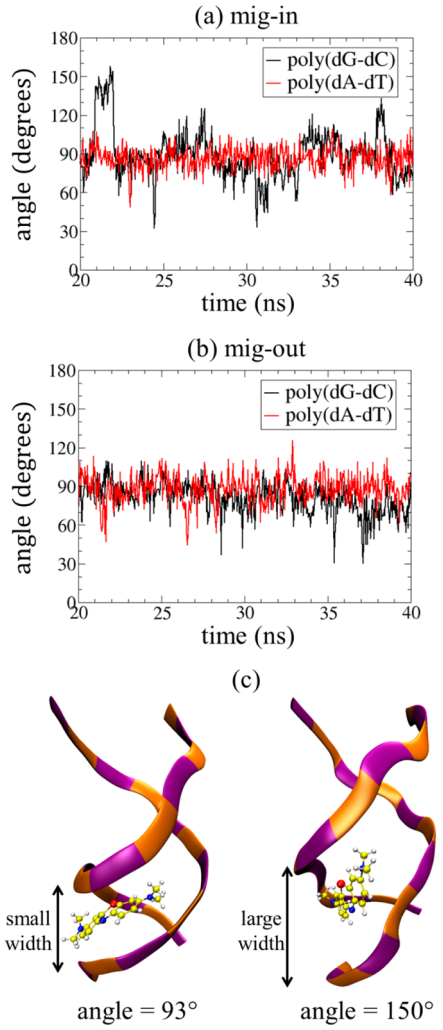

Figure 7. Time evolution of the angle formed by the short axis of MB v_{short}(MB) and the helical axis of DNA v_{helix} for the (a) mig-in and (b) mig-out orientations in both DNA sequences at ionic strength 1.0 M. (c) Snapshots taken from the simulations which show the relation between the MB rotation and the minor groove width.

but they are implicitly described into the Coulomb and van der Waals potential terms. Recent MD simulations[43,45] have employed the same force field (GAFF+bsc0/ff99) to investigate the intercalative binding mode of doxorubicin,[45] rhodamine 6G, and QSY 21.[43] The binding modes extracted from these simulations resemble the structures found by NMR and X-ray experiments. In addition, our simulated binding energies also agree with the experimental findings. Thus, the applicability of the AMBER force field to the study of drug−DNA intercalative binding is supported by all these data.

As discussed in the Binding Energies section, the variation of binding energies with the DNA sequence and the ionic strength mimic the experimental behavior. However, the binding energies of intercalative complexes must be examined carefully because several transitions between symmetric and gauche orientations take place during the dynamics. Scheme 3 lists the symmetric/gauche transitions for all the intercalative initial conditions.

Since the strength of the intermolecular MB/DNA and intramolecular DNA interactions changes with the dye orientation inside the binding pocket, the evaluation of the binding energy depends on the simulation fragment that is

dx.doi.org/10.1021/bi500068z | Biochemistry 2014, 53, 2391−2412

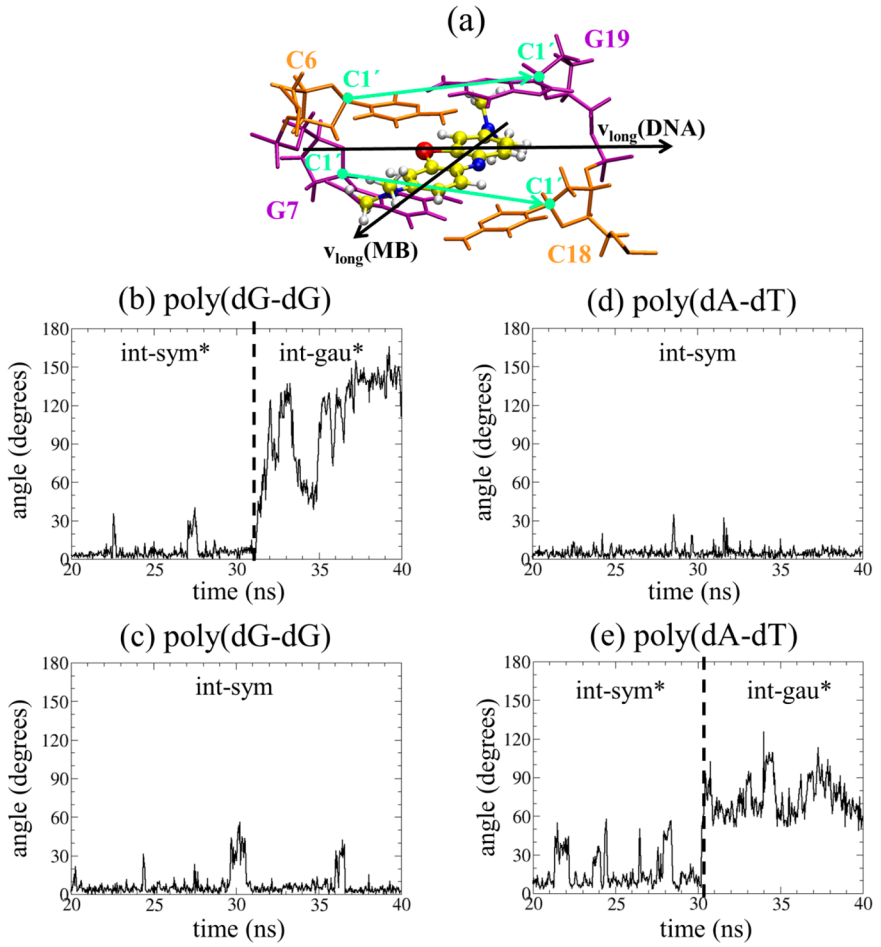

Figure 8. (a) Representation of the long axis of MB v_{long}(MB) and the average long axis of the flanking base pairs v_{long}(DNA). Time evolution of the angle formed by v_{long}(MB) and v_{long}(DNA) for (b) poly(dG-dC) with initial geometry int-sym at ionic strength 0 M, (c) poly(dG-dC) with initial geometry int-gau at ionic strength 0 M, (d) poly(dA-dT) with initial geometry int-sym at ionic strength 0 M, and (e) poly(dA-dT) with initial geometry int-gau at ionic strength 0 M. Color atoms and residues: yellow for C, blue for N, red for S, white for H, purple for guanine, and orange for cytosine.

Table 8. Binding Free Energy Decomposition (kcal/mol) into MB Deformation Energy E_{def} (MB), DNA Deformation Energy E_{def} (DNA), Intermolecular Energy E_{inter} (MB/DNA) and Nonpolar Solvation Energy $\Delta G_{nonpolar}$ for Intercalative Complexes at Ionic Strength 0 M

	poly(dG-dC)			poly(dA-dT)		
initial structure	int-sym		int-gau	int-gau	int-gau	
MD structure[a]	int-sym*	int-gau*	int-sym	int-sym	int-sym*	int-gau*
E_{def} (MB)	4.7	5.2	4.9	5.4	5.7	6.9
E_{def} (DNA)	31.4	30.9	25.0	25.3	29.3	34.1
E_{inter} (MB/DNA)	−55.0	−53.6	−55.6	−54.2	−49.7	−54.6
$\Delta G_{nonpolar}$	8.3	9.2	7.6	10.0	9.9	13.4
binding energy[b]	−10.6	−8.3	−18.1	−13.5	−4.8	−0.2

[a]The geometries int-sym come from simulations without rotational transitions and int-sym* and int-gau* from simulations with rotational transitions. [b]The standard error of the mean for all binding energies is ∼0.6 kcal/mol.

being analyzed. Thus, for example, if the energy calculation is performed over the last 28 ns (instead 20 ns), the MB/poly(dG-dC) binding energy for the int-gau initial structure at ionic strength 0 M changes from −18.1 to −15.7 kcal/mol (see Table 4). If one examines the transitions listed in Scheme 3 for these conditions, the decrease in the binding energy can be readily rationalized. During the last 20 ns of the simulation, the dye lies in the symmetric configuration all the time. However, during the last 28 ns, the system adopts the gauche geometry in part of the simulation, and the binding energy is lower for the gauche intercalative binding mode for mainly two reasons: (i) the π-stacking interactions between MB and the flanking base pairs are partially broken for gauche geometries; (ii) the DNA deformation energy is larger for gauche configurations (see below). Thus, a more accurate evaluation of the binding energy would require too many longer simulations to have a large number of symmetric/gauche transitions and therefore better statistics of the structural configurations.

dx.doi.org/10.1021/bi500068z | *Biochemistry* 2014, 53, 2391−2412

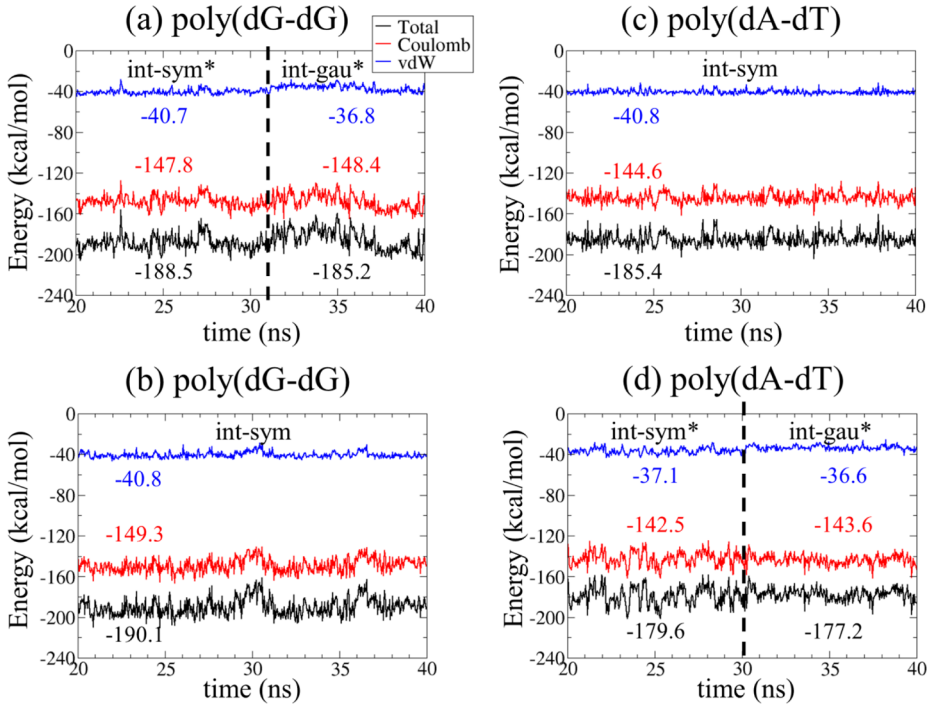

Figure 9. Time evolution of the gas-phase interaction energy between MB and the flanking base pairs (black line) and its Coulomb E_{Coul} (MB/DNA) (red line) and van der Waals E_{vdW} (MB/DNA) (blue line) contributions for (a) poly(dG-dC) with initial geometry int-sym at ionic strength 0 M, (b) poly(dG-dC) with initial geometry int-gau at ionic strength 0 M, (c) poly(dA-dT) with initial geometry int-sym at ionic strength 0 M, and (d) poly(dA-dT) with initial geometry int-gau at ionic strength 0 M. The values into the plots are the average energies in kcal/mol.

Scheme 3 shows that for two trajectories at ionic strength 0 M (initial geometry int-gau for GC and initial geometry int-sym for AT) the dye lies in the symmetric orientation during the last 20 ns of the simulation. For the other two trajectories (initial geometry int-sym for GC and initial geometry int-gau for AT), MB undergoes a transition from the symmetric to gauche orientation over the last 20 ns of simulation. The rotation of MB inside the intercalative pocket may be followed throughout the dynamics by calculating the angle formed by the long axis of MB ν_{long}(MB) and the averaged long axis of the two flanking base pairs ν_{long}(DNA). We have placed the dye into the base pair steps 5′-C6-G7-3′ for GC and 5′-T6-A7-3′ for AT. The average long axis of the C6-G19 and G7-C18 (or T6-A19 and A7-T18) flanking base pairs was approximated as the average of the vectors that connect the C1′ atoms of the sugars of each nucleoside in the base pair. The definition of the axes is displayed in Figure 8a for poly(dG-dC), and the variation of the angle formed by the ν_{long}(MB) and ν_{long}(DNA) vectors for the GC and AT sequences at ionic strength 0 M is represented in Figure 8b−e. The transitions from int-sym to int-gau are clearly identified at 31 and 30 ns.

The energy decomposition according to eqs 5−8 for the trajectories at ionic strength 0 M is listed in Table 8. For each nucleic acid, we found two symmetric orientations with different energetic features depending on the simulation that is analyzed, that is, simulation with or without transition over the last 20 ns. To differentiate the two situations, we will refer to the symmetric structure of the simulation without transitions as int-sym (without asterisk) and to the symmetric and gauche structures of the simulations with transition as int-sym* and int-gau* (with asterisk).

a. Most Stable Structures for poly(dG-dC) and poly(dA-dT). Table 8 shows the binding energy decomposition into E_{def} (MB), E_{def} (DNA), E_{inter} (MB/DNA), and $\Delta G_{nonpolar}$ for the three complex structures found in the simulations, that is, int-sym, int-sym*, and int-gau*. The strongest binding energy was observed for the int-sym geometry for both DNA sequences (−18.1 kcal/mol for GC and −13.5 kcal/mol for AT). The examination of the energy contributions for the int-sym orientation indicates that the binding energy difference between GC and AT is mainly due to a larger unfavorable nonpolar solvation energy $\Delta G_{nonpolar}$ and a less attractive MB/DNA interaction E_{inter} (MB/DNA) for AT. The deformation energy of the dye (4.9 kcal/mol for GC vs 5.4 kcal/mol for AT) and nucleic acid structures (25.0 kcal/mol for GC and 25.3 kcal/mol for AT) is similar for both sequences.

E_{inter} (MB/DNA) can be expressed as the sum of E_{gas} (MB/DNA) and the polar solvation energy ΔG_{polar} (MB/DNA), according to eq 8. In turn, E_{gas} (MB/DNA) includes the interaction between the dye and the 24 nucleosides of the simulated DNA; however, the most important interactions are observed between MB and the flanking nucleosides. The time evolution of the MB/C6-G19-G7-C18 and MB/T6-A19-A7-T18 gas-phase interactions and the Coulomb and van der Waals contributions for the simulations at low salt concentration is presented in Figure 9. The interaction between the dye and the flanking base pairs for int-sym is −190.1 kcal/mol for GC and −185.4 kcal/mol for AT. Interestingly, the value of the van der Waals term is the same for both sequences (−40.8 kcal/mol). The energy difference lies in the Coulomb contribution (−149.3 kcal/mol for GC vs −144.6 kcal/mol for AT).

The nonpolar contribution of the solvation energy $\Delta G_{nonpolar}$ must be also taken into account to explain the differences in the binding energies between the int-sym orientations of the two DNA sequences. $\Delta G_{nonpolar}$ is 7.6 kcal/mol for poly(dG-dC)

dx.doi.org/10.1021/bi500068z | *Biochemistry* 2014, 53, 2391−2412

Table 9. Nonpolar Solvation Energy $\Delta G_{nonpolar}$ Decomposition (kcal/mol) into Repulsion ΔG_{rep} and Dispersion ΔG_{disp} Energies of the MB-DNA Complex and the Isolated MB and DNA Molecules for Intercalative Complexes at Ionic Strength 0 M

	poly(dG-dC)			poly(dA-dT)		
initial structure	int-sym		int-gau	int-sym	int-gau	
MD structure[a]	int-sym*	int-gau*	int-sym	int-sym	int-sym*	int-gau*
ΔG_{rep} (MB − DNA)	495.4	497.4	496.2	511.4	510.9	509.6
ΔG_{rep} (MB)	33.6	33.6	33.6	33.6	33.6	33.6
ΔG_{rep} (DNA)	476.6	476.6	476.5	492.8	493.4	492.1
ΔG_{rep}	−14.8	−12.8	−13.9	−15.0	−16.1	−16.1
ΔG_{disp} (MB − DNA)	−454.4	−455.5	−455.8	−455.9	−455.3	−450.5
ΔG_{disp} (MB)	−33.5	−33.3	−33.5	−33.5	−33.5	−33.5
ΔG_{disp} (DNA)	−443.6	−444.2	−443.8	−447.4	−447.8	−446.5
ΔG_{disp}	23.1	22.0	21.5	25.0	26.0	29.5
$\Delta G_{nonpolar}$	8.3	9.2	7.6	10.0	9.9	13.4

[a]The geometries int-sym come from simulations without rotational transitions and int-sym* and int-gau* from simulations with rotational transitions.

and 10.0 kcal/mol for poly(dA-dT). As explained in the section of computational details, $\Delta G_{nonpolar}$ is the sum of a positive energy ΔG_{rep} that describes the solute−solvent repulsive interactions and the formation of the solute cavity, and a favorable energy resulting from dispersion attractive interactions ΔG_{disp} between solute and solvent molecules.[41] Each of these terms is computed as the difference between the energy of the adduct and the energy of the unbound DNA and MB; that is, $\Delta G_{rep(disp)} = \Delta G_{rep(disp)}$ (MB − DNA) $-\Delta G_{rep(disp)}$ (*DNA*) − $\Delta G_{rep(disp)}$ (MB). The values of these contributions are listed in Table 9. The total repulsive term ΔG_{rep} is −13.9 and −15.0 kcal/mol for GC and AT, respectively, but the dispersion interaction ΔG_{disp} shows more significant differences between GC (21.5 kcal/mol) and AT (25.0 kcal/mol). The principal reason of this discrepancy is the fact that the dispersion interaction between the free double strand and the solvent is more attractive for poly(dA-dT) (−447.4 kcal/mol) than for poly(dG-dC) (−443.8 kcal/mol). Therefore, when the dye is noncovalently bound to DNA, the loss of stability is more important for the AT sequence.

b. Comparison of Symmetric Structures. Two different symmetric structures (int-sym and int-sym*) were found in the simulations for each DNA sequence with important differences in energetic and structural properties. In the case of poly(dG-dC), the binding energy (Table 8) between the two orientations differs by 7.7 kcal/mol (−10.6 kcal/mol for int-sym* and −18.1 kcal/mol for int-sym), while for poly(dA-dT) the difference is 8.7 kcal/mol (−4.8 kcal/mol for int-sym* and −13.5 for int-sym). Therefore, the int-sym orientation is the most favorable binding mode for both sequences. The reasons that explain this behavior will be discussed in the following paragraphs.

We will start comparing the energy decomposition of Table 8 for the int-sym and int-sym* geometries of poly(dG-dC). The main discrepancy between both structures is observed in the intramolecular deformation of DNA. E_{def} (DNA) is 31.4 kcal/mol for int-sym* and 25.0 kcal/mol for int-sym. Therefore, the double strand is less stable for the symmetric structure of the simulation with the symmetric/gauche transition. All the intra- and interbase pair rotational and translational parameters, the total helical axis bend, and the width of the minor and major grooves were computed for int-sym and int-sym* and are shown in Table S1 of the Supporting Information. These parameters were defined elsewhere.[35] The values for the free nucleic acids are also included for comparison. All the DNA structural parameters were calculated at the 5′-C6-G7-3′ and 5′-T6-A7-3′ level for GC and AT, respectively, and for the computation of the total helical axis bend the first and the last base pairs were excluded. As can be seen in Table S1, there is not a clear correlation between the structural parameters and E_{def} (DNA). This means that the variation of some parameters leads to more important energy changes than others. In this case, the higher E_{def} (DNA) for int-sym* is likely related with the larger X-displacement of the base pairs (2.33 Å for int-sym* and 1.55 Å for int-sym) and with the larger widening of the minor groove (3.46 Å for int-sym* and 2.56 Å for int-sym) with respect to the free poly(dG-dC).

The interaction energy between MB and poly(dG-dC) E_{inter} (MB/DNA) is similar for both int-sym (−55.0 kcal/mol) and int-sym* (−55.6 kcal/mol) orientations. To get more insight into the dye/DNA interactions, the time evolution of the MB/C6-G19-G7-C18 gas-phase interactions and the Coulomb and van der Waals contributions plotted in Figures 9a (int-sym*) and 9b (int-sym) can be compared. The total gas-phase interaction between MB and the flanking nucleosides of poly(dG-dC) for both symmetric structures is very similar (−190.1 kcal/mol for int-sym and −188.5 kcal/mol for int-sym*). This result is in agreement with the angular behavior observed in Figure 8b,c. The angle formed by v_{long}(MB) and v_{long}(DNA) is nearly zero virtually the whole time for both symmetric structures. Few angular deviations from the ideal value of 0° are detected. Therefore, this similar alignment between the dye and the flanking base pairs for both symmetric orientations provide similar interaction energies.

If the same analysis of the int-sym and int-sym* geometries is performed for the AT sequence at ionic strength 0 M the trends are more evident. Table 8 shows that the stronger binding energy found for int-sym is explained by a more attractive E_{inter} (MB/DNA) (−54.2 kcal/mol for int-sym vs −49.7 kcal/mol for int-sym*) and a smaller E_{def} (DNA) (25.3 kcal/mol for int-sym vs 29.3 kcal/mol for int-sym*). The variation of the DNA structural parameters after complexation is represented in Table S2 of the Supporting Information. In that case, the large increment of the total helical axis bend with respect to the free helix is clearly the dominant parameter. This increment is 14.6 Å for int-sym and 32.8 Å for int-sym*.

The stronger attraction E_{inter} (MB/DNA) between MB and poly(dA-dT) for the int-sym orientation is explained attending

dx.doi.org/10.1021/bi500068z | *Biochemistry* 2014, 53, 2391−2412

to the orientation of the dye inside the intercalative pocket. The value of the angle formed by v_{long}(MB) and v_{long}(DNA) is near zero most of the simulation time only for the int-sym orientation (Figure 8d). In contrast, many MB rotations between 0 and 50° are observed for the int-sym* geometry (Figure 8e). This large deviation from the ideal value of 0° reduces the alignment between the dye and the flanking basis-pairs, and therefore, E_{inter} (MB/DNA) decreases. This can be corroborated by examining the time evolution of the MB/T6-A19-A7-T18 gas-phase interaction depicted in Figure 9c,d. The total interaction energy is −185.4 kcal/mol for int-sym and −179.6 kcal/mol for int-sym*. Both van der Waals (−40.8 kcal/mol for int-sym and −37.1 kcal/mol for int-sym*) and Coulomb (−144.6 kcal/mol for int-sym and −142.5 kcal/mol for int-sym*) energies are more attractive for the int-sym configuration. Therefore, the angular orientation of MB is responsible for the observed energy differences.

c. Analysis of Symmetric/Gauche Transitions. The symmetric/gauche transitions can be characterized by comparing the int-sym* and int-gau* orientations for each DNA sequence. The differences between the binding energies (Table 8) are 2.3 kcal/mol for GC (−10.6 kcal/mol for int-sym* and −8.3 kcal/mol for int-gau*) and 4.6 kcal/mol for AT (−4.8 kcal/mol for int-sym* and −0.2 kcal/mol for int-gau*). These energy differences are well above the thermal energy (kT); therefore, one could suspect that the transitions observed in the trajectories are the result of some artifact of the simulation. However, the approximations that have been used to compute the binding energies must be considered. First, the entropy term of eq 2 was neglected. This term will likely be very similar for int-sym* and int-gau* but in any case not completely the same. Second, and most important, the simulations were run employing the explicit TIP3P model for the solvent while the binding energy was calculated with the implicit Poisson−Boltzmann model. Therefore, the solvation energy term introduces discrepancies between the real binding energy of the simulation and the binding energy computed with the implicit model. Probably, the energy differences between the int-sym* and int-gau* orientations are smaller than those shown here. Keeping in mind these limitations, the rotational transitions will be examined below.

Regarding poly(dG-dC), the energy decomposition of Table 8 reveals that any of the energy terms is clearly the responsible of the larger binding energy of int-sym*. E_{def} (MB), E_{inter} (MB/DNA), and $\Delta G_{nonpolar}$ are more favorable for int-sym* by 0.5, 1.4, and 0.9 kcal/mol, respectively, while E_{def} (DNA) is smaller for int-gau* by 0.5 kcal/mol. The variation of the DNA structural parameters after the binding of MB shown in Table S1 agrees with the small E_{def} (DNA). For example, the change in X-displacement (2.33 Å for int-sym* vs 1.11 Å for int-gau*), twist (38.4° for int-sym* vs 16.0° for int-gau*), minor groove width (3.46 Å for int-sym* vs 2.56 Å for int-gau*), or major groove width (4.49 Å for int-gau* vs 3.76 Å for int-gau*) destabilizes the helix in the int-sym* geometry to a greater extent than in int-gau*. However, other structural parameters such as shift (0.13 Å for int-sym* vs 0.40 Å for int-gau*), slide (0.21 Å for int-sym* vs 1.0 Å for int-gau*), and rise (3.33 Å for int-sym* vs 3.56 Å for int-gau*) are less energetically favorable for the int-gau* orientation. Therefore, the different deformations counteract one another resulting in a small DNA deformation energy difference between both structures (0.5 kcal/mol). Regarding E_{def} (MB), any significant difference was detected between int-sym* and int-gau*. In general, the deformation of the dye consists of out-of-plane motions for both orientations.

E_{inter} (MB/DNA) is the energy contribution that presents the largest difference (1.4 kcal/mol) between int-sym* and int-gau*. The gas-phase interaction between MB and the bases C6, G19, G7, and C18 plotted in Figure 9a follows the expected behavior; that is, the attractive interaction energy is larger for int-sym* (−188.5 kcal/mol) than for int-gau* (−185.2 kcal/mol) due to the better alignment of the aromatic rings of the dye and nucleic bases in the int-sym geometry (Figure 8a).

The nonpolar contribution of the solvation energy $\Delta G_{nonpolar}$ must be also taken into account to explain the small differences between the binding energies of the symmetric and gauche configurations of poly(dG-dC). $\Delta G_{nonpolar}$ is 8.3 kcal/mol for int-sym* and 9.2 kcal/mol for int-gau*. The different contributions of $\Delta G_{nonpolar}$ appear in Table 9. For poly(dG-dC), the values of the repulsive and dispersion energies that come from the unbound DNA and MB monomers are very similar for int-sym* and int-gau*. The main differences come from the contribution of the MB-DNA complex. ΔG_{rep} (MB − DNA) is 2.0 kcal/mol more energetically disfavorable for int-gau*, while ΔG_{disp} (MB − DNA) is 1.5 kcal/mol more energetically favorable for int-gau*. Therefore, in global the nonpolar solvation energy is slightly more repulsive for the int-gau* orientation.

The different energy terms that contribute to the binding energy show more important differences between int-sym* and int-gau* for the AT sequence as seen in Table 8. E_{def} (DNA) is 29.3 kcal/mol for int-sym* and 34.1 kcal/mol for int-gau*. This difference of 4.8 kcal/mol can be mostly attributed to the variation of the total helical axis bend (Table S2, Supporting Information). Increments of 32.8 Å and 41.7 Å with respect to the free polynucleotide were computed for int-sym* and int-gau*, respectively. In addition, important structural variations were also found in the rise separation (3.80 Å for int-sym* vs 4.09 Å for int-gau*) and the shift distance (0.25 Å for int-sym* vs 2.20 Å for int-gau*).

Unlike for poly(dG-dC), the intermolecular energy E_{inter} (MB/DNA) between the dye and the AT sequence is 4.9 kcal/mol more attractive for int-gau* (−54.6 kcal/mol) than for int-sym* (−49.7 kcal/mol). However, the gas-phase interaction between MB and the T6, A19, A7, T18 bases shows the regular time evolution trend (Figure 9d), that is, more attraction for the int-sy m* geometry. Values of −179.6 and −177.2 kcal/mol were computed for the int-sym* and int-gau* orientations, respectively. Therefore, the stabilization of E_{inter} (MB/DNA) for int-gau* is due to the interaction between the dye and nucleotides placed farther than the flanking base pairs.

Table 9 shows that $\Delta G_{nonpolar}$ also presents large discrepancies between both geometries. The most unfavorable nonpolar solvation energy is present in the gauche orientation (as for the GC sequence), but in this case the difference between the symmetric (9.9 kcal/mol) and gauche (12.4 kcal/mol) geometries is more important. The total repulsive terms ΔG_{rep} have the same value for the two configurations (−16.1 kcal/mol), while the larger dispersion interaction between the MB/DNA complex and the solvent for int-sym* makes the total dispersion term ΔG_{disp} less unfavorable for the symmetric (26.0 kcal/mol) than for the gauche (29.5 kcal/mol) structure.

In summary, symmetric/gauche transitions were detected in our simulations. The previous analysis concludes that the int-sym* orientation is more stable than the int-gau* one. A

complex balance among the different energy contributions is necessary to explain the different behaviors of both structures. The symmetric configurations analyzed in the Major Groove Binding section (int-sym) are more stable than the int-sym* orientations of the present section. In addition, rotational transitions from int-sym (and not from int-sym*) were not predicted for the simulations. This indicates that the system could adopt several intermediate states when symmetric/gauche transitions take place. More accurate methods are necessary to perform a more quantitative analysis of the rotational transitions. A quantum mechanics/molecular mechanics (QM/MM) investigation is planned in this direction.

d. Intercalation at High Ionic Strength. At ionic strength 1.0 M, symmetric intercalation is still the most abundant binding mode for poly(dG-dC) as can be seen in Scheme 3. However, the dynamics is significantly different for poly(dA-dT). The dye lies in the pocket with the gauche orientation virtually the whole simulation time. This situation does not allow a detailed analysis of symmetric/gauche transitions as was performed for the dynamics at low ionic strength, but still interesting conclusions can be obtained.

The decomposition of the binding energy (eqs 5−8) for the trajectories at ionic strength 1.0 M is shown in Table 10.

Table 10. Binding Free Energy Decomposition (kcal/mol) into MB Deformation Energy E_{def} (MB), DNA Deformation Energy E_{def} (DNA), Intermolecular Energy E_{inter} (MB/DNA) and Nonpolar Solvation Energy $\Delta G_{nonpolar}$ for Intercalative Complexes at Ionic Strength 1.0 M

	poly(dG-dC)		poly(dA-dT)	
initial structure	int-sym	int-gau	int-sym	int-gau
MD structure	int-sym	int-sym/int-gau[a]	int-gau	int-gau
E_{def} (MB)	5.6	5.5	6.0	5.5
E_{def} (DNA)	25.5	23.0	26.9	28.9
E_{inter} (MB/DNA)	−54.7	−52.8	−52.3	−51.2
$\Delta G_{nonpolar}$	7.1	6.0	10.5	8.3
binding energy[b]	−16.5	−18.3	−8.9	−8.5

[a]The int-gau orientation is observed only during 1.5 ns in the last 20 ns of simulation. [b]The standard error of the mean for all binding energies is ∼0.6 kcal/mol.

Comparison with the results of Table 8 (ionic strength 0 M) provides interesting conclusions, especially for poly(dA-dT). The binding strength of the gauche intercalative binding mode for AT increases from −0.2 kcal/mol at ionic strength 0 M to −8.9 and −8.5 kcal/mol (for initial geometries int-sym and int-gau, respectively) at ionic strength 1.0 M. This stabilization of the gauche orientation is a consequence of a large relaxation of the double strand. E_{def} (DNA) decreases from 34.1 to 26.9 kcal/mol and 28.9 kcal/mol when increasing the salt concentration. Structural analysis reveals that the main variation in the DNA structure happens in the total helical axis bend. The change with respect the free DNA is 41.7° at ionic strength 0 M (Table S2) and 7.9° and 24.0° for the simulations at ionic strength 1.0 M with initial geometries int-sym and int-gau, respectively.

In addition, the relaxation of the helix also causes strong variations in the nonpolar solvation energy. $\Delta G_{nonpolar}$ drops from 13.4 kcal/mol (Table 8) to 10.5 and 8.3 kcal/mol (Table 10) for the simulations with initial geometries int-sym and int-gau, respectively, with increasing the salt concentration. The decomposition of $\Delta G_{nonpolar}$ at high ionic strength (not shown for simplicity) reveals that dispersion energy between the MB/DNA adduct and the solvent is more attractive at ionic strength 1.0 M (−456.5 and −455.7 kcal/mol for initial geometries int-sym and int-gau, respectively) than that at ionic strength 0 M (−450.5 kcal/mol). Therefore, the decrease of the helical axis bend induces favorable dispersion interactions between the complex and the solvent.

Since the binding energy of the gauche intercalative mode for AT (−8.9 kcal/mol and −8.5 kcal/mol) is similar to that of the minor groove mode (−8.8 kcal/mol) as can be seen in Table 4, both configurations can be present at high ionic strength for poly(dA-dT). Experimental analyses[12] have found two different binding modes for poly(dA-dT) at high salt concentration. One of them was the intercalative binding mode and the other could not be resolved from the spectroscopic measurements. However, it was suggested to be the major groove binding. Our simulations explain the two different structures observed experimentally. However, our analyses reveal that the minor groove complex is the second structure.

The decrease of the binding energy of the intercalative interaction mode due to the rotation of the dye from the symmetric to gauche configuration inside the binding pocket with the increase of ionic strength explains the experimental findings. This rotation of MB inside the intercalative pocket was proposed previously based on spectroscopic measurements.[9]

CONCLUSIONS

In this work, we have investigated using force field MD simulations the binding modes by which MB can noncovalently bind to two different DNA sequences. In particular, external, intercalative and minor and major groove bindings were analyzed for alternating GC and AT sequences at ionic strengths 0 and 1.0 M.

External binding complexes were found to be unstable structures which dissociate or migrate to other binding site during the simulations. The interaction time between the dye and the phosphate groups extracted from the time evolution of the number of interatomic contacts is in the range between 300 ps and 2.7 ns. The external binding mode is dominated by Coulomb interactions. Around the 93% (78%) of the MB/DNA total gas-phase interaction energy for GC (AT) comes from the Coulomb contribution.

The major groove binding simulations did not provide stable adducts for the GC sequence. The formation of hydrogen bonds between the NH_2 groups of the guanine nucleotides and the aromatic N atom of MB is important at high ionic strength. Hydrogen bonding is present over the 36% and 19% of the interaction time for the simulations with initial geometry mag-in and mag-out, respectively, at ionic strength 1.0 M. This contributes to the stabilization of the system and results in longer MB/poly(dG-dC) interaction times (∼4 ns) compared to the external binding. However, the complexes dissociated for the four different initial conditions analyzed here. Therefore, it is concluded that the major groove binding mode is not favorable for the GC sequence.

For poly(dA-dT) the dye interacts with the helix inside the major groove over the whole simulation time for three of the four trajectories investigated. Hydrogen bond lifetimes are longer than those for the GC sequence. At ionic strength 0 M the formation of hydrogen bonds is observed during the 32% of the simulation. This percentage increases up to 52% (initial geometry mag-in) and 76% (initial geometry mag-out) at ionic

strength 1.0 M. However, the MB/DNA complexes are characterized by high mobility of the dye inside the major groove, indicating that a stable energy minimum was not achieved. Nevertheless, the formation of major groove adducts for the AT sequence should not be ruled out, especially at high ionic strengths.

Minor groove MB/DNA adducts are stable structures for both DNA sequences. Coulomb interactions represent more than the 90% of the MB/DNA total gas-phase interaction energy. Our simulations predict different features of the minor groove binding for the two DNA sequences. For poly(dG-dC) the minor groove complex is energetically favored when the dimethylamino groups of the dye faces outside the groove (mig-out), while in the MB/poly(dA-dT) complex the orientation with the dimethylamino groups oriented toward the groove (mig-in) is the most stable structure.

For both DNA sequences the number of interatomic contacts is larger for the mig-in orientation than for the mig-out one, which results in more attractive MB/DNA van der Waals and Coulomb interactions. However, the steric effect in the mig-in orientation produced by the NH_2 groups inside the minor groove for poly(dG-dC) makes the MB/DNA interactions less important than for poly(dA-dT). This smaller interaction energy in the GC sequence is not able to counteract the DNA deformation energy, and therefore the balance between the different energy contributions makes the mig-out orientation the most stable structure for poly(dG-dC).

The mig-out configuration favors hydrogen bond formation in the GC sequence between the aromatic N atom of MB and the NH_2 group of one of the guanine residues during the 90% of the simulation. However, this hydrogen bond does not play an important role in the formation of mig-out adducts since the MB/DNA gas-phase interaction energy is stronger for the mig-in orientation. Hydrogen bonding is not possible for the AT sequence because of the absence of hydrogen donors inside the minor groove.

The minor groove binding induces a narrowing of the minor groove except for the GC sequence at high ionic strength where the minor groove is broadened. This is explained by the high mobility of the dye inside the groove for these conditions, likely due to the strong interaction between the dye and the ions of the environment.

Intercalation is the most important binding mode found in the simulations. Three different structures were observed during the dynamics. Two of them present a parallel orientation with respect to the aromatic system of the flanking base-pair (int-sym and int-sym*) and the other is rotated by more than 60° around the helical axis (int-gau*). Transitions between int-sym* and int-gau* orientations take place throughout the dynamics.

At ionic strength 0 M, the strongest binding energy was computed for the int-sym orientation for both DNA sequences. The int-sym complex was found to be more stable for the GC sequence (−18.1 kcal/mol) than for the AT sequence (−13.5 kcal/mol). This energy difference mainly comes from the discrepancies in the attractive gas-phase Coulomb interaction between MB and the flanking base pairs (−149.3 kcal/mol for GC and −144.6 kcal/mol for AT) and the dispersion contribution of the nonpolar solvation energy (21.5 kcal/mol for GC and 25.0 kcal/mol for AT).

The two symmetric geometries (int-sym and int-sym*) detected at low ionic strength in the simulations show different characteristics. Binding energies are clearly more favorable for the int-sym orientation (−18.1 and −13.5 kcal/mol for GC and AT, respectively) than those for the int-sym* orientation (−10.6 and −4.8 kcal/mol for GC and AT, respectively). The int-sym complex in the GC sequence is more stable due to the smaller DNA deformation energy (25.0 kcal/mol) compared to int-sym* (31.4 kcal/mol). In the case of poly(dA-dT), both the DNA deformation energy (25.3 and 29.3 kcal/mol for int-sym and int-sym*, respectively) and gas-phase interaction between MB and the flanking base pairs (−185.4 and −179.6 kcal/mol for int-sym and int-sym*, respectively) play an important role in the stabilization of the int-sym configuration.

Transitions between the int-sym* and int-gau* orientations were analyzed for GC and AT at ionic strength 0 M. Binding energies of −10.6 kcal/mol (GC) and −4.8 kcal/mol (AT) were computed for int-sym*, while values of −8.3 kcal/mol (GC) and −0.2 kcal/mol (AT) were obtained for int-gau*. However, this greater stability of int-sym* over int-gau* could be overestimated due to the approaches employed to compute the binding energies. A complex balance among the deformation energies of MB and DNA, MB/DNA interaction energy and solvation energy is necessary to explain the trends observed for the int-sym* and int-gau* structures.

At high ionic strength the symmetric intercalation is still dominant for poly(dG-dC), but the gauche intercalation is the only configuration observed for poly(dA-dT). The decrease of the variation of the total helical axis bend with respect to the free AT sequence from 41.7° to 7.9° and 24.0° (for initial geometries int-sym and int-gau, respectively) induces an energetically stabilization of the double strand and favors more attractive dispersion interactions between the adduct and the solvent. The comparable binding energies of the gauche intercalative (−8.9 and −8.5 kcal/mol) and minor groove (−8.8 kcal/mol) structures for AT suggest the existence of both binding modes at ionic strength 1.0 M. These findings agree with the two different binding modes found in the experiments[12] for the AT sequence at high ionic strength.

■ ASSOCIATED CONTENT

Ⓢ Supporting Information

MB force field parameters in prmtop format, RMSD plots, and DNA structural parameters. This material is available free of charge via the Internet at http://pubs.acs.org.

■ AUTHOR INFORMATION

Corresponding Author

*E-mail: nogueira.perez.juanjose@univie.ac.at. Phone: +43 1 4277 52765.

Funding

The present work was supported by the Marie Curie Actions-Intra-European Fellowships, call FP7-PEOPLE-2012-IEF, through the project PHOTOBLUE (Project Number 327412).

Notes

The authors declare no competing financial interest.

■ REFERENCES

(1) Hurley, L. H. (2002) DNA and its associated processes as targets for cancer therapy. *Nat. Rev. Cancer 2* (3), 188−200.

(2) Gurova, K. (2009) New hopes from old drugs: Revisiting DNA-binding small molecules as anticancer agents. *Future Oncol. 5* (10), 1685−1704.

(3) David-Cordonnier, M. H., Laine, W., Lansiaux, A., Rosu, F., Colson, P., de Pauw, E., Michel, S., Tillequin, F., Koch, M., Hickman, J. A., Pierré, A., and Bailly, C. (2005) Covalent binding of antitumor

benzoacronycines to double-stranded DNA induces helix opening and the formation of single-stranded DNA: Unique consequences of a novel DNA-bonding mechanism. *Mol. Cancer Ther. 4* (1), 71−80.
(4) Strekowski, L., and Wilson, B. (2007) Noncovalent interactions with DNA: An overview. *Mutat. Res., Fundam. Mol. Mech. Mutagen. 623* (1−2), 3−13.
(5) Ihmels, H., and Otto, D. (2005) Intercalation of Organic dye molecules into double-stranded DNA - General principles and recent developments. *Top. Curr. Chem. 258*, 161−204.
(6) Gao, Q., Williams, L. D., Egli, M., Rabinovich, D., Chen, S. L., Quigley, G. J., and Rich, A. (1991) Drug-induced DNA repair: X-ray structure of a DNA-ditercalinium complex. *Proc. Natl. Acad. Sci. U.S.A. 88* (6), 2422−2426.
(7) Banerjee, D., and Pal, S. K. (2008) Dynamics in the DNA recognition by DAPI: Exploration of the various binding modes. *J. Phys. Chem. B 112* (3), 1016−1021.
(8) Müller, W., and Crothers, D. M. (1975) Interactions of heteroaromatic compounds with nucleic acids. I. The influence of heteroatoms and polarizability on the base specificity of intercalating ligands. *Eur. J. Biochem. 54* (1), 267−277.
(9) Nordén, B., and Tjerneld, F. (1982) Structure of methylene blue-DNA complexes studied by linear and circular dichroism spectroscopy. *Biopolymers 21* (9), 1713−1734.
(10) Tong, C., Hu, Z., and Wu, J. (2010) Interaction between methylene blue and calfthymus deoxyribonucleic acid by spectroscopic technologies. *J. Fluoresc. 20* (1), 261−267.
(11) Tuite, E., and Kelly, J. M. (1995) The interaction of methylene blue, azure B, and thionine with DNA: Formation of complexes with polynucleotides and mononucleotides as model systems. *Biopolymers 35* (5), 419−433.
(12) Tuite, E., and Nordén, B. (1994) Sequence-specific interactions of methylene blue with polynucleotides and DNA: A spectroscopic study. *J. Am. Chem. Soc. 116* (17), 7548−7556.
(13) Zhang, L. Z., and Tang, G. Q. (2004) The binding properties of photosensitizer methylene blue to herring sperm DNA: A spectroscopic study. *J. Photochem. Photobiol., B 74* (2−3), 119−125.
(14) Mellish, K. J., Cox, R. D., Vernon, D. I., Griffiths, J., and Brown, S. B. (2002) In vitro photodynamic activity of a series of methylene blue analogues. *Photochem. Photobiol. 75* (4), 392−397.
(15) Orth, K., Russ, D., Beck, G., Rück, A., and Beger, H. G. (1998) Photochemotherapy of experimental colonic tumours with intratumorally applied methylene blue. *Langenbecks Arch. Surg. 383* (3−4), 276−281.
(16) Orth, K., Ruck, A., Stanescu, A., and Beger, H. G. (1995) Intraluminal treatment of inoperable oesophageal tumours by intralesional photodynamic therapy with methylene blue [12]. *Lancet 345* (8948), 519−520.
(17) Zolfaghari, P. S., Packer, S., Singer, M., Nair, S. P., Bennett, J., Street, C., and Wilson, M. (2009) In vivo killing of Staphylococcus aureus using a light-activated antimicrobial agent. *BMC Microbiol. 9*, 27.
(18) Ragàs, X., Dai, T., Tegos, G. P., Agut, M., Nonell, S., and Hamblin, M. R. (2010) Photodynamic inactivation of Acinetobacter baumannii using phenothiazinium dyes: In vitro and in vivo studies. *Lasers Surg. Med. 42* (5), 384−390.
(19) Phillips, D. (2011) Toward targeted photodynamic therapy. *Pure Appl. Chem. 83* (4), 733−748.
(20) O'Connor, A. E., Gallagher, W. M., and Byrne, A. T. (2009) Porphyrin and nonporphyrin photosensitizers in oncology: Preclinical and clinical advances in photodynamic therapy. *Photochem. Photobiol. 85* (5), 1053−1074.
(21) Tanielian, C., and Wolff, C. (1995) Determination of the parameters controlling singlet oxygen production via oxygen and heavy-atom enhancement of triplet yields. *J. Phys. Chem. 99* (24), 9831−9837.
(22) Cotes Oyaga, S., Cotua Valdes, J., Borja Paez, S., and Hurtado Marquez, K. (2013) DFT Description of Intermolecular Forces between 9-Aminoacridines and DNA Base Pairs. *J. Theor. Chem. 2013*, No. 526569.
(23) Rohs, R., Sklenar, H., Lavery, R., and Röder, B. (2000) Methylene blue binding to DNA with alternating GC base sequence: A modeling study. *J. Am. Chem. Soc. 122* (12), 2860−2866.
(24) Rohs, R., and Sklenar, H. (2004) Methylene Blue Binding to DNA with Alternating AT Base Sequence: Minor Groove Binding is Favored over Intercalation. *J. Biomol. Struct. Dyn. 21* (5), 699−711.
(25) Rohs, R., and Sklenar, H. (2001) Methylene blue binding to DNA with alternating GC base sequence: Continuum treatment of salt effects. *Indian J. Biochem. Biophys. 38* (1−2), 1−6.
(26) Rohs, R., Bloch, I., Sklenar, H., and Shakked, Z. (2005) Molecular flexibility in ab initio drug docking to DNA: Binding-site and binding-mode transitions in all-atom Monte Carlo simulations. *Nucleic Acids Res. 33* (22), 7048−7057.
(27) Spink, N., Brown, D. G., Skelly, J. V., and Neidle, S. (1994) Sequence-dependent effects in drug-DNA interaction: The crystal structure of Hoechst 33258 bound to the d(CGCAAATTTGCG)2 duplex. *Nucleic Acids Res. 22* (9), 1607−1612.
(28) Case, D. A.; Darden, T. A.; Cheatham III, T. E.; Simmerling, C. L.; Wang, J.; Duke, R. E.; Luo, R.; Walker, R. C.; Zhang, W.; Merz, K. M.; Roberts, B.; Hayik, S.; Roitberg, A.; Seabra, G.; Swails, J.; Götz, A. W.; Kolossváry, I.; Wong, K. F.; Paesani, F.; Vanicek, J.; Wolf, R. M.; Liu, J.; Wu, X.; Brozell, S. R.; Steinbrecher, T.; Gohlke, H.; Cai, Q.; Ye, X.; Wang, J.; Hsieh, M.-J.; Cui, G.; Roe, D. R.; Mathews, D. H.; Seetin, M. G.; Salomon-Ferrer, R.; Sagui, C.; Babin, V.; Luchko, T.; Gusarov, S.; Kovalenko, A.; Kollman, P. A. (2012) *AMBER 13*, University of California, San Francisco.
(29) Jorgensen, W. L., Chandrasekhar, J., Madura, J. D., Impey, R. W., and Klein, M. L. (1983) Comparison of simple potential functions for simulating liquid water. *J. Chem. Phys. 79* (2), 926−935.
(30) Phillips, J. C., Braun, R., Wang, W., Gumbart, J., Tajkhorshid, E., Villa, E., Chipot, C., Skeel, R. D., Kalé, L., and Schulten, K. (2005) Scalable molecular dynamics with NAMD. *J. Comput. Chem. 26* (16), 1781−1802.
(31) Wang, J., Wolf, R. M., Caldwell, J. W., Kollman, P. A., and Case, D. A. (2004) Development and testing of a general Amber force field. *J. Comput. Chem. 25* (9), 1157−1174.
(32) Wang, J., Cieplak, P., and Kollman, P. A. (2000) How Well Does a Restrained Electrostatic Potential (RESP) Model Perform in Calculating Conformational Energies of Organic and Biological Molecules? *J. Comput. Chem. 21* (12), 1049−1074.
(33) Pérez, A., Marchán, I., Svozil, D., Sponer, J., Cheatham, T. E., III, Laughton, C. A., and Orozco, M. (2007) Refinement of the AMBER force field for nucleic acids: Improving the description of α/γ conformers. *Biophys. J. 92* (11), 3817−3829.
(34) Frisch, M. J.; Trucks, G. W.; Schlegel, H. B.; Scuseria, G. E.; Robb, M. A.; Cheeseman, J. R.; Scalmani, G.; Barone, V.; Mennucci, B.; Petersson, G. A.; Nakatsuji, H.; Caricato, M.; Li, X.; Hratchian, H. P.; Izmaylov, A. F.; Bloino, J.; Zheng, G.; Sonnenberg, J. L.; Hada, M.; Ehara, M.; Toyota, K.; Fukuda, R.; Hasegawa, J.; Ishida, M.; Nakajima, T.; Honda, Y.; Kitao, O.; Nakai, H.; Vreven, T.; Montgomery, J. A., Jr.; ; Peralta, J. E.; Ogliaro, F.; Bearpark, M.; Heyd, J. J.; Brothers, E.; Kudin, K. N.; Staroverov, V. N.; Kobayashi, R.; Normand, J.; Raghavachari, K.; Rendell, A.; Burant, J. C.; Iyengar, S. S.; Tomasi, J.; Cossi, M.; Rega, N.; Millam, N. J.; Klene, M.; Knox, J. E.; Cross, J. B.; Bakken, V.; Adamo, C.; Jaramillo, J.; Gomperts, R.; Stratmann, R. E.; Yazyev, O.; Austin, A. J.; Cammi, R.; Pomelli, C.; Ochterski, J. W.; Martin, R. L.; Morokuma, K.; Zakrzewski, V. G.; Voth, G. A.; Salvador, P.; Dannenberg, J. J.; Dapprich, S.; Daniels, A. D.; Farkas, Ö.; Foresman, J. B.; Ortiz, J. V.; Cioslowski, J.; Fox, D. J. (2013) *Gaussian 09*, Revision D.01, Gaussian, Inc., Wallingford CT.
(35) Lavery, R., Moakher, M., Maddocks, J. H., Petkeviciute, D., and Zakrzewska, K. (2009) Conformational analysis of nucleic acids revisited: Curves+. *Nucleic Acids Res. 37* (17), 5917−5929.
(36) Humphrey, W., Dalke, A., and Schulten, K. (1996) VMD: Visual molecular dynamics. *J. Mol. Graphics 14* (1), 33−38.
(37) Roe, D. R., and Cheatham, T. E. (2013) PTRAJ and CPPTRAJ: Software for processing and analysis of molecular dynamics trajectory data. *J. Chem. Theory Comput. 9* (7), 3084−3095.

(38) Srinivasan, J., Cheatham, T. E., III, Cieplak, P., Kollman, P. A., and Case, D. A. (1998) Continuum solvent studies of the stability of DNA, RNA, and phosphoramidate-DNA helices. *J. Am. Chem. Soc. 120* (37), 9401−9409.
(39) Kollman, P. A., Massova, I., Reyes, C., Kuhn, B., Huo, S., Chong, L., Lee, M., Lee, T., Duan, Y., Wang, W., Donini, O., Cieplak, P., Srinivasan, J., Case, D. A., and Cheatham, T. E., III (2000) Calculating structures and free energies of complex molecules: Combining molecular mechanics and continuum models. *Acc. Chem. Res. 33* (12), 889−897.
(40) Miller, B. R., III, McGee, T. D., Swails, J. M., Homeyer, N., Gohlke, H., and Roitberg, A. E. (2012) MMPBSA.py: An efficient program for end-state free energy calculations. *J. Chem. Theory Comput. 8* (9), 3314−3321.
(41) Tan, C., Tan, Y. H., and Luo, R. (2007) Implicit nonpolar solvent models. *J. Phys. Chem. B 111* (42), 12263−12274.
(42) Homeyer, N., and Gohlke, H. (2012) Free energy calculations by the Molecular Mechanics Poisson-Boltzmann Surface Area method. *Mol. Informatics 31* (2), 114−122.
(43) Kabeláč, M., Zimandl, F., Fessl, T., Chval, Z., and Lankaš, F. (2010) A comparative study of the binding of QSY 21 and Rhodamine 6G fluorescence probes to DNA: Structure and dynamics. *Phys. Chem. Chem. Phys. 12* (33), 9677−9684.
(44) Zhao, G. C., Zhu, J. J., and Chen, H. Y. (1999) Spectroscopic studies of the interactive model of methylene blue with DNA by means of *β*-cyclodextrin. *Spectrochim. Acta, Part A 55* (5), 1109−1117.
(45) Lei, H., Wang, X., and Wu, C. (2012) Early stage intercalation of doxorubicin to DNA fragments observed in molecular dynamics binding simulations. *J. Mol. Graph. Model. 38*, 279−289.
(46) Ramachandran, S., Temple, B., Alexandrova, A. N., Chaney, S. G., and Dokholyan, N. V. (2012) Recognition of platinum-DNA adducts by HMGB1a. *Biochemistry 51* (38), 7608−7617.